https://doi.org/10.5194/egusphere-2026-2773
Preprint. Discussion started: 15 July 2026

Multi-year characterization of low volatility vapors in a boreal forest

Chengfeng Liu[1], Otso Peräkylä[1,2], Lauri Ahonen[1], Ilona Ylivinkka[1], Petri Keronen[1], Douglas R. Worsnop[1,3], Tuukka Petäjä[1], Markku Kulmala[1], Mikael Ehn[1] & Nina Sarnela[1]

[1]Institute for Atmospheric and Earth System Research/Physics, Faculty of Science, University of Helsinki, Helsinki, 00014, Finland
[2]Nanjing-Helsinki Institute in atmospheric and Earth System Sciences, Nanjing University, Suzhou, 210008, China
[3]Aerodyne Research, Billerica, MA 01821, USA

Correspondence to: Nina Sarnela (nina.sarnela@helsinki.fi)

Abstract. Atmospheric low volatility vapors play an essential role in aerosol particle formation, growth, and cloud condensation nuclei production, thereby influencing climate. While intensive measurements have been carried out in different locations, little is known about their seasonal variability due to a lack of long-term measurements. To address this gap, we present nearly 4 years of continuous observations of low volatility vapors in a boreal forest measured using a NO_3^- atmospheric pressure interface time-of flight (MION-Api-TOF) mass spectrometer. Our results reveal the seasonal variation in the concentration, molecular composition, formation mechanism and volatility distribution of highly oxygenated organic molecules (HOMs). We show that while temperature-dependent terpene emissions regulate the overall seasonal abundance of HOMs, distinct formation pathways govern their diurnal profiles: monoterpene-derived monomers peak during the day due to the availability of precursors and oxidants, whereas their dimers peak at night driven by low concentrations of terminating species (NO and HO_2) and extended RO_2 radical lifetimes. We observed differing seasonal changes across different HOMs species and, although C_{10} HOMs remains the dominant HOM species during the whole year, sesquiterpene-derived C_{15} HOMs shows the steepest increase during summer. Using binned Nonnegative Matrix Factorization (bin-NMF), we found that HOM composition is strongly modulated by seasonality. While monoterpene-derived HOMs containing nitrogen atoms ("CHON") dominate during colder months, summertime chemistry is characterized by a shift toward "CHO" species and a substantial contribution from heavy terpenes (sesquiterpenes and diterpenes), which can account for 40%-80% of the signal in the high-mass range (m/z 450–700, including NO_3^-). We also analysed the seasonal volatility distribution of HOMs and identified the primary contributors to each volatility class. Crucially, challenging the long-held assumption that monoterpene derived C_{17-20} HOM dimers are the most important biogenic precursors of new particle formation in the boreal forest, we found sesquiterpene-derived C_{13-15} HOMs and C_{17-20} HOMs have comparable contribution to Ultra-Low Volatility Organic Compounds (ULVOCs) during daytime throughout much of the year. Moreover, in spring -- the season with the highest NPF frequency at our measurement site, sesquiterpene-derived C_{13-15} HOM account for approximately 40% of ULVOC during daytime, compared to 28 % for C_{17-20} HOMs. Our findings provide critical new insights into the seasonal dynamics of HOM composition and their broader atmospheric implications.

https://doi.org/10.5194/egusphere-2026-2773
Preprint. Discussion started: 15 July 2026

1 Introduction

Atmospheric aerosols can affect global climate, air quality, and human health. More than 60% of the aerosol number load and more than 50% of the cloud condensation nuclei are estimated to be contributed by new particle formation (NPF) (Kulmala, 2025). For the past decades, a variety of aerosol precursors have been found in different environments, including sulfuric acid, organics, ammonia, amine and iodine oxoacids (Kirkby et al., 2023; Zhao et al., 2024).

The role of organic compounds in particle formation has received increasing attention since 2002, when organics, produced by oxidation of terpenes released from trees were found to be the main composition of 3-5nm particles in the forest (O'Dowd et al., 2002). The first observation of highly oxygenated organic molecules (HOMs) was conducted in a boreal forest in 2010 (Ehn et al., 2010), and then a similar mass spectrum was detected in a chamber study on monoterpene ozonolysis two years later, confirming the gaseous formation of HOMs from monoterpenes (Ehn et al., 2012), and the link between HOMs and nucleation and particle growth was found in the next year (Zhao et al., 2013). In 2013, Crounse et al. (2013) found a rapid oxidation process under atmospherically relevant conditions, termed autoxidation. Subsequently, Ehn et al. (2014) demonstrated that autoxidation can proceed through multiple sequential steps within a single molecule, generating substantial amounts of highly oxygenated organic molecules (HOMs) from biogenic volatile vapors. Those HOMs are usually characterized by low to extremely low volatility and hence capable of enhancing, or even dominating, new particle formation and growth in the forest. This finding sparked a wave of studies, revealing this previously overlooked mechanism as a key player in NPF, secondary organic aerosol formation and cloud formation under various environments. (Bianchi et al., 2019; Kulmala et al., 2013; Lai et al., 2024; Petäjä et al., 2022; Riccobono et al., 2014; Roldin et al., 2019; Schobesberger et al., 2013; Tröstl et al., 2016; Zha et al., 2024).

In detail, autoxidation is a sequential oxidation process starting from peroxy radicals (RO_2), which are usually formed by the oxidation of VOCs by OH, O_3, or NO_3. In autoxidation, the RO_2 undergo intramolecular H-shifts followed by O_2 addition to reform a new RO_2. This process allows RO_2 to have rapid increase of oxidation level with simultaneous decrease of volatility, which will finally be terminated, forming a close-shelled product, via intramolecular rearrangement causing the loss of e.g. OH or HO_2, or via biomolecular reactions with HO_2, NO_x or other RO_2. Globally, VOCs are emitted in large quantities from vegetation (Wang et al., 2024a). Among those, an important and abundant group of VOCs, terpenes, have been found to be efficient in forming HOMs (Bianchi et al., 2019; Jokinen et al., 2016; Luo et al., 2022). If a HOM molecule is formed from a monoterpene ($C_{10}H_{16}$), then it usually has 10 or 20 carbon atoms, although the final product might lose one or several carbons (Kang et al., 2025; Peräkylä et al., 2023; Pullinen et al., 2020). This enables us to infer the precursors of the detected HOMs from their elemental composition. Since the regional disparities are large, the produced HOMs are also different in different areas. Monoterpenes are the most abundantly emitted biogenic volatile organic vapors in the boreal forest (Rantala et al., 2015). Combining with their relatively high HOM yields (Bianchi et al., 2019), this leads to the formula of detected HOMs usually being $C_{9-10}H_{15-17}N_{0-2}O_z$ and $C_{18-20}H_{30-32}N_{0-2}O_z$ (Ehn et al., 2012). As a contrast, oxygenated organic molecules with mainly 4-5 carbon atoms have been observed in the free troposphere over Amazonia, where isoprene (C_5H_8) emissions dominate

https://doi.org/10.5194/egusphere-2026-2773
Preprint. Discussion started: 15 July 2026

(Curtius et al., 2024; Shen et al., 2024; Zha et al., 2024). Simultaneously, despite the fact that emissions and the atmospheric abundance of sesquiterpenes are usually 1-2 orders of magnitude lower than isoprene (Li et al., 2020; Wang et al., 2024a), their oxidation products can still have an important contribution to HOMs formation due to their high reactivities. (Isaacman-VanWertz et al., 2024; Jokinen et al., 2016). Barreira et al. (2021) found, in the hemi boreal forest, that the oxidation products of sesquiterpenes were the predominant fraction in the particle phase during part of the time although the measured concentration of sesquiterpene oxidation products in the gas phase is still lower than monoterpenes. It should be noted that the yield of HOM and the yield of secondary organic aerosol (SOA) vary for different terpenes. Although the concentrations of heavier terpenes (e.g. sesquiterpenes, diterpenes) are much lower than the concentration of monoterpene, their contribution to aerosols might be underestimated, considering their high reactivity with O_3 and high mass yield of SOA (Atkinson and Arey, 2003; Barreira et al., 2021; Hellén et al., 2018; Liu et al., 2024; Luo et al., 2022). In the atmosphere, different terpenes are mixed, interacting with each other and causing even more complicated cross reactions and HOM yields (Dada et al., 2023).

In addition to the precursors, there are also other factors significantly affecting the yields and composition of HOMs. NO_x plays a complex role in terminating autoxidation chains. Generally it reduces HOM yields since the reaction with NO_x competes with autoxidation reaction and it can terminates the reaction chain before RO_2 reaches high oxygen number (Liu et al., 2021; Yan et al., 2020). However, it has been shown that under low- NO regime, NO can enhance the HOMs formation by modulating the RO_2 loss and favoring the formation of alkoxy radicals that can continue to autoxidize through isomerization (Nie et al., 2023). Fragmentation is also found to be increased under high NO_x level, leading to the formation of HOMs with fewer carbon atoms (Pullinen et al., 2020). HO_2 radicals, as one of the most important daytime radicals, are reported to suppress HOMs production and shift HOMs monomer functionalization from carbonyl to hydroperoxide (Baker et al., 2024). Temperature mainly influences the H-shift rate which is the limiting step for autoxidation (Praske et al., 2018). As a result, HOM yields are supposed to increase with temperature since bimolecular termination is only weakly related to temperature (Ziemann and Atkinson, 2012). The decreasing of HOM yields under lower temperatures has been verified recently, but how temperature impacts HOM composition is still unclear (Frege et al., 2018; Luo et al., 2024; Quéléver et al., 2019; Stolzenburg et al., 2018).

Previous studies on HOMs have largely relied on short-term field campaigns, while long-term measurements remain scarce, due to the fact that it's very challenging to provide persistent maintenance and support to the instrument. In the context of global warming and declining NO_x emissions, the role of HOMs in SOA formation and climate feedback is expected to increase. The absence of long-term observations limits a comprehensive evaluation of the potential of HOMs to form SOA and their broader climate impacts. Extended datasets, spanning years or even decades, are essential to address key questions such as how HOM concentrations and compositional distributions evolve under changing environmental conditions. In addition, the short-term measurement can't provide information about the influence of large-scale perturbations, such as the COVID-19 pandemic or forest management activities.

Although some intermediate-term studies have been conducted, they still fall short of providing a complete picture as often HOMs are presented as a sum of all compounds (Neefjes et al., 2022) or as few tracers of different type of HOM (Sulo et al.,

https://doi.org/10.5194/egusphere-2026-2773
Preprint. Discussion started: 15 July 2026

2021). Jokinen et al. (2022a) reported a 7-month measurement, revealing the seasonal variation of sulfuric acid, iodine acid, methanesulfonic acid and HOMs, showing a strong temperature dependence of HOMs concentration. However, no molecular composition of HOMs were shown. Guo et al. (2022) investigated the seasonal variation of oxygenated organic molecules with the highest concentration also in summer, based on a 135-day measurement around the year of 2019.

In this study, we present, to the best of our knowledge, the longest continuous NO_3-CIMS measurement of low-volatility vapors to date (2019.2–2022.11), with a focus on the seasonal variation of HOM concentrations, molecular composition, formation mechanism and volatility distributions. We first examine the links between HOM behavior and environmental conditions, then analyse the compositional distributions and apply a factorization method to classify HOM species. Based on these results, we identify the main HOM chemistry in the boreal forest throughout the year and discuss its implications. Finally, we report the volatility distributions of HOMs across seasons.

2 Methods

2.1 Instrumentation

The core instrument for this study is a multi-scheme chemical ionization atmospheric pressure interface time-of-flight (MION-APi-TOF; Karsa Ltd., Finland) mass spectrometer. The MION inlet is capable of fast switching between multiple reagent ion schemes, allowing us to measure a more complete range of oxygenated molecules in the atmosphere (Huang et al., 2021; Rissanen et al., 2019). The reagent ion precursors are charged by soft X-rays and then guided through an orifice into the laminar sample flow by electric field within the ion source. A small counterflow is also added to prevent uncharged reagent ion precursors from entering the sample gas. Compared to the commonly used Eisele inlet (Eisele and Tanner, 1993), the perpendicular design of the sample gas and electric streamlines, along with the electric field inside the ionization source, enhances the reagent ion transport efficiency from the ion source to the pinhole of the TOF (Finkenzeller et al., 2024).

The MION-APi-TOF has been deployed for continuous measurement at the SMEAR II station (Hyytiälä, 61.8417° N, 24.2896° E) with two ionization schemes (nitrate and bromide) since 2019. The measurements in different modes are performed in 1-hour cycles, which consist of 30 min for ambient ions, 12 min for the NO_3^- mode, 12 min for the Br^- mode and, followed by 6 min pf ion-filter zeroing before proceeding to the next cycle. In this study, we restricted our analysis to data derived via NO_3^- ionization, given our focus on low-volatility compounds. Additionally, only data from February 2019 to November 2022 are included, as processing a longer dataset is highly time-consuming and a technical malfunction induced a calibration factor shift in late November 2022. Despite instrument issues that caused gaps in this dataset, it still covers significantly more data than earlier studies and therefore provides a more representative characterization of HOMs across all seasons.

We also measured monoterpenes, the main precursors of HOMs at the SMEAR II station, using a quadrupole proton transfer reaction mass spectrometer (PTR-MS) (Taipale et al., 2008). The instrument sampled air at various heights from the bottom to the top of a mast. In this study, only measurement from the lowest height (4.2 m) was used, as the MION-APi-TOF was

https://doi.org/10.5194/egusphere-2026-2773
Preprint. Discussion started: 15 July 2026

located at ground level. In addition, monoterpenes, sesquiterpenes and diterpenes were measured with a Vocus PTR-TOF-MS from Apr. 2022 to Nov. 2022 at a height of 35 m on the measurement tower.

2.2 Quantification of low volatility vapors

The instrument was calibrated using a sulfuric acid (SA) calibrator as described by Kürten et al.(2012). The instrument was calibrated in August 2022 and a calibration coefficient of 8.6 x 10^9 was applied to the entire study period for calculating atmospheric SA concentrations. In practice, the calibration coefficient is unlikely to remain stable over multiple years. It can, in principle, fluctuate due to changing environmental conditions, drift gradually due to instrument aging, and shift abruptly in response to hardware malfunctions or significant changes in instrument performance. To investigate this uncertainty, we evaluated the ratio of measured SA to its calculated proxy, alongside the estimated yield of a representative HOM ($C_{10}H_{14}O_7$) over the study period. As shown in Fig S1, although the measured-to-proxy SA ratio fluctuated by three orders of magnitude, and the $C_{10}H_{14}O_7$ yield by two orders of magnitude, there was no clear long-term trend or sudden discontinuity over the first four years. However, on November 25, 2022, the ionization source was cleaned, which noticeably altered the instrument's performance. Consequently, data collected after this date were excluded from this study to ensure consistency. Because a robust interannual analysis would require more frequent (e.g., monthly) calibrations to accurately track instrument performance, we do not draw conclusions regarding year-to-year trends of low-volatility vapors. Furthermore, the fluctuations observed over the four years should not be interpreted solely as measurement uncertainty. These variations also stem from uncertainties in the SA proxy calculation and natural seasonal shifts in temperature, precursor concentrations, and terminating species that affect nighttime $C_{10}H_{14}O_7$ formation.

For HOMs, the presence of thousands of compounds makes it impossible to determine individual calibration factors for each one. A widely used approach, also adopted in this study, is to apply a uniform calibration factor to all HOMs, based on the assumption that they are charged at the kinetic limit similarly to sulfuric acid (Ehn et al., 2014). The concentration of HOMs was calculated as shown in Eq. (1).

$$[HOM] = \frac{HOM(NO_3^-)}{\sum_{i=0}^{2}(HNO_3)_i(NO_3^-)} \times C, \quad (1)$$

where [HOM] is the concentration (cm^{-3}) of the HOM molecules to be calculated. These molecules are identified through high-resolution peak fitting of each nominal mass. $HOM(NO_3^-)$ and $(HNO_3)_iNO_3^-$ are the signals (ions/s) of the target HOM molecule sand reagent ions detected by the MION-APi-TOF, respectively. C is the SA calibration factor (molecules $\cdot cm^{-3} \cdot$ s $\cdot$ $count^{-1}$). However, it is important to recognize the uncertainty associated with this assumption and the limited number of calibrations. In addition, because these measurements were obtained during the early years of operation without a transmission calibration, mass-dependent transmission further contributes to the overall measurement uncertainty. Overall, we estimated the uncertainties to be ± 200% and ± 600% for the measurement of SA and HOMs, respectively.

The MION-APi-TOF data were processed using Tofware (version 3.3.0), one month at a time. The length of the data processing period needs to be carefully chosen since the mass calibration, peak width and shape are expected to drift with time. In our

https://doi.org/10.5194/egusphere-2026-2773
Preprint. Discussion started: 15 July 2026

case, a test was conducted before choosing the processing period by processing the data on a weekly and monthly basis separately and comparing their peak widths and shapes (Fig S2). According to the results, we concluded that the small weekly shift in the peak width and shape would not affect the accuracy of peak fitting.

The HOM volatility was estimated based on the parameterization by Mohr et al. (2019) and further corrected using ambient temperature. Based on their saturation mass concentration (C_{sat}), organic compounds are usually divided into ultra-low-volatility organic compounds (ULVOCs), extremely low-volatility organic compounds (ELVOCs), low-volatile organic compounds (LVOCs) and semi-volatile organic compounds (SVOCs). These classes correspond to C_{sat} ranges of $< 10^{-8.5}$, $10^{-8.5}$ to $10^{-4.5}$, $10^{-4.5}$ to $10^{-0.5}$ and $10^{-0.5}$ to $10^{2.5}$ μg m^{-3}, respectively

2.3 Binned Nonnegative Matrix Factorization (bin-NMF)

A bin-PMF (positive matrix factorization) method was previously reported for aiding peak fitting and data interpretation (Zhang et al., 2019). In this method, the mass spectra are divided into narrow bins after mass calibration, and then the bins are used as inputs for factorization. In our study, we introduced several modifications to the published method. First, because the peak width increases linearly with mass, a stepwise increasing bin width was applied, ensuring a fixed number of bins per peak across the entire mass range (seven bins per peak in this study). Second, instead of selecting the binning region within each nominal mass, the full mass spectra were first binned, after which noise bins were removed using a threshold based on the spectral noise level. This approach significantly reduced the number of bins used as the input and improved the computational efficiency of the factorization. Finally, non-negative matrix factorization (NMF) was employed in place of PMF, as it is computationally much more efficient and readily implemented in Python via the scikit-learn library (https://scikit-learn.org/stable/modules/generated/sklearn.decomposition.NMF.html).

The core difference between the two methods lies in their optimization approaches and treatment of observational error. PMF minimizes a specialized objective function that utilizes a comprehensive uncertainty matrix to evaluate signal-to-noise ratios, mathematically down-weighting unreliable measurements so they do not distort the underlying factor profiles. While such an uncertainty matrix is often critical for integrated atmospheric measurements, its application to CI-APi-TOF data presents a distinct scenario. As demonstrated by Yan et al. (2016) , who proposed two approaches to estimate this uncertainty from experimental and ambient data, the electronic noise level across the mass spectrum is generally assumed to be uniform. Consequently, uncertainty primarily arises from Poisson counting statistics, which depend only on ion signals. Because measurement error is uniformly and deterministically tied to signal intensity across the entire mass spectrum, the dataset largely lacks the sporadic, species-specific analytical errors that PMF's uncertainty matrix is explicitly designed to penalize, making the unweighted approach of NMF mathematically viable. Furthermore, while PMF explicitly relies on the "n_runs" parameter to perform dozens of random initializations to guarantee convergence on a mathematically stable global minimum, standard NMF algorithms typically execute a single run using a deterministic initialization, which carries the risk of converging on a local minimum. However, the primary objective of utilizing NMF in this study is exploratory feature extraction from a massive dataset, rather than strict physical source apportionment. To validate this approach, we evaluated the model's performance by

https://doi.org/10.5194/egusphere-2026-2773
Preprint. Discussion started: 15 July 2026

calculating the reconstruction error between the measured and NMF-output signals, ensuring that the extracted latent features successfully capture the dominant chemical variance of our dataset. Ultimately, given the large dataset and the need for computational efficiency and methodological accessibility, we selected NMF as our factorization tool for this study.

3 Results and discussion

3.1 Time series, seasonal and diurnal variations of sulfuric acid and HOMs

The overall data coverage of the dataset is 65%, reflecting the challenges of operating the instrument continuously, especially during the early years with the original MION inlet design. During the first three years, the most frequent issue occurred in summer, when pollen entered the ionization source and interfered with the measurements. In April 2022, the inlet was modified by adding a purge flow to the ionization source to prevent sample air from entering directly. This improvement substantially enhanced measurement stability, increasing the data coverage for the last year to 89%. Despite these challenges, this dataset remains the most extensive NO_3^--APi-TOF dataset to date and should provide a representative characterization of SA and HOMs across all four seasons, as it spans nearly four years.

The majority of the compounds investigated in this study possess an oxygen number greater than six, aligning with the standard definition of HOMs (Bianchi et al., 2019). HOMs were classified into seven groups -- $C_{7\text{-}10}H_yO_z$, $C_{7\text{-}10}$ RO_2, $C_{7\text{-}10}H_yO_zN_{1\text{-}2}$, $C_{17\text{-}20}H_yO_z$, $C_{17\text{-}20}H_yO_zN_{1\text{-}2}$, Other $C_{<20}H_yO_z(N)$ and Other $C_{\geq 20}H_yO_z(N)$. The detailed classification method is provided in Table S1. We used carbon numbers of 10 and 20, as monoterpenes ($C_{10}H_{16}$) are the dominant precursors in Hyytiälä, and the corresponding HOM monomers and dimers are expected to contain 10 and 20 carbon atoms, respectively. Considering that the oxidation process often leads to some loss of carbon atoms (Peräkylä et al., 2023; Pullinen et al., 2020), carbon ranges of $C_{7\text{-}10}$ and $C_{17\text{-}20}$ were used. However, caution is required when associating these groups directly with monoterpene-derived HOMs, as other volatile organic compounds (VOCs) may contribute to the same groups, albeit at lower fractions. For instance, isoprene-isoprene HOM dimers share the same chemical formula as monoterpenes HOM monomers, while monoterpene-monoterpene (MT-MT) HOM dimers may overlap with diterpene HOM monomers. The "CHON" monomer and dimer groups, $C_{7\text{-}10}H_yO_zN_{1\text{-}2}$ and $C_{17\text{-}20}H_yO_zN_{1\text{-}2}$, include compounds containing either 1 or 2 nitrogen atoms. The HOMs that did not fall into any of the above-mentioned groups were divided based on their carbon number into two groups, Other $C_{<20}H_yO_z(N)$ and Other $C_{\geq 20}H_yO_z(N)$. These groups include molecules both with and without nitrogen. Note that these two groups contain 464 and 121 species, respectively—a combined total that surpasses that of monoterpene-derived HOMs. Previously, compounds in these groups have received less attention because monoterpenes have been assumed to be the dominant HOM precursors in boreal forests. However, their total concentrations are comparable to, or even exceed, those of the corresponding monoterpene-derived groups, highlighting their potential atmospheric importance.

In this section, we first present the characteristic seasonal patterns and diurnal cycles of SA and HOM concentrations in different groups and investigate how these variations relate to key environmental drivers. We then proceed to a more detailed, compound-level analysis to understand the compositional changes underlying the temporal variation of HOM groups.

https://doi.org/10.5194/egusphere-2026-2773
Preprint. Discussion started: 15 July 2026

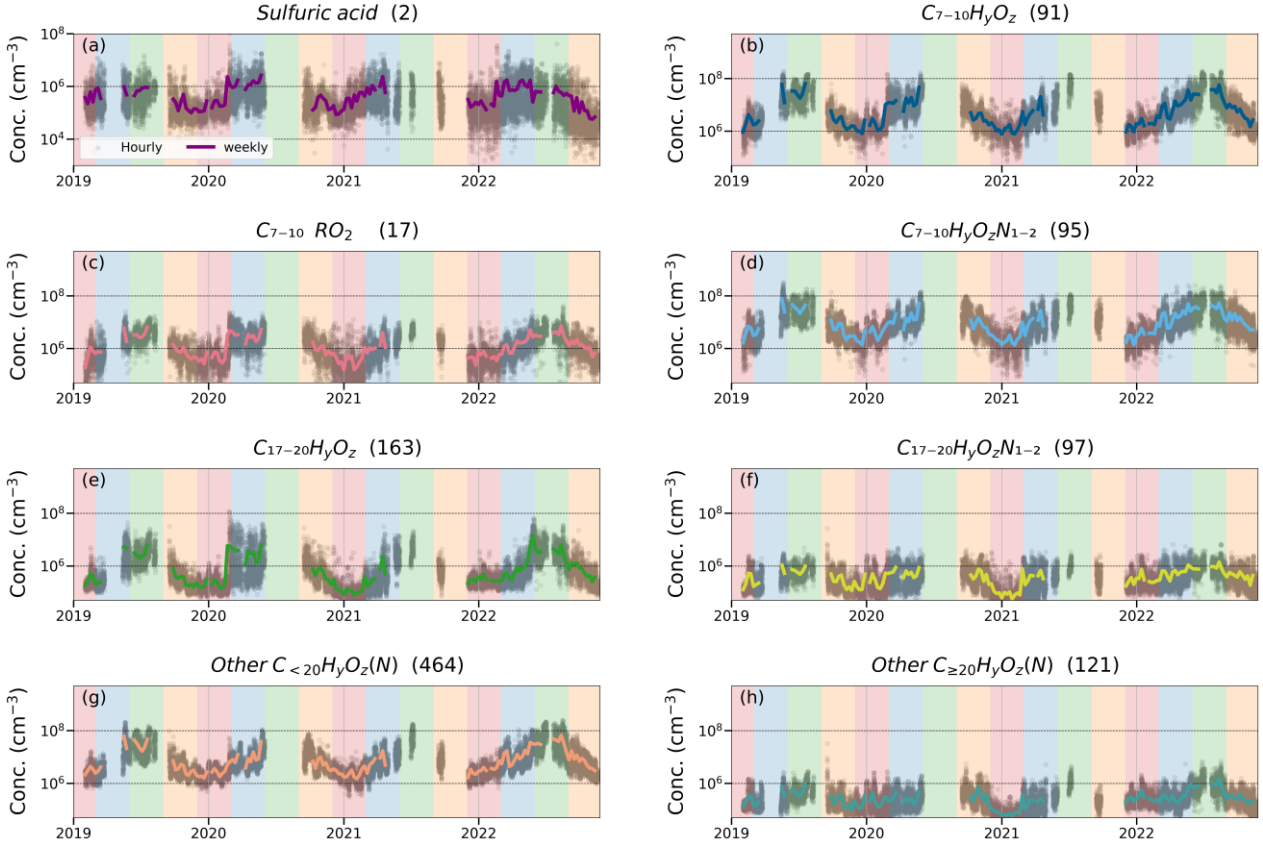

Figure 1: Time series of measured low-volatility vapors: (a) sulfuric acid; (b) $C_{7-10}H_yO_z$; (c) C_{7-10} RO_2 radicals; (d) $C_{7-10}H_yO_zN$; (e) $C_{17-20}H_yO_z$; (f) $C_{17-20}H_yO_zN$; (g) other $C_{<20}H_yO_z(N)$; (h) other $C_{\geq 20}H_yOz(N)$. Numbers in parentheses indicate the number of peaks included in each group. The season is defined as follows: blue, spring (Mar.-May); green, summer (Jun.-Aug.), orange, fall (Sep.-Nov.) and red, winter (Dec.–Feb.).The classification method is described in detail in Table S1.

The time series of sulfuric acid and the seven HOM subgroups are shown in Fig. 1. In general, all low-volatility compounds exhibited similar seasonal patterns, reaching their maximum concentrations during the warm season. For SA, considered the primary nucleation driver in Hyytiälä (Lehtipalo et al., 2018), the weekly mean concentration typically varied between 1×10^5 and 1×10^7 cm^{-3}. Excluding the Other $C_{<20}H_yO_z(N)$ and Other $C_{\geq 20}H_yO_z(N)$ groups, $C_{7\text{-}10}H_yO_z$ and $C_{7\text{-}10}H_yO_zN_{1\text{-}2}$ were the most abundant HOM subgroups, with weekly concentrations ranging from 1×10^6 to 1×10^8 cm^{-3}. These observations suggest that reactive nitrogen chemistry may play an important role in HOM formation in Hyytiälä, even though the median NO concentration is 0.04 ppb (5^{th}-95^{th} percentiles: 0.00-0.17 ppb) throughout the year. Yan et al. (2016) also found that NO played an important role in Hyytiälä during late spring of 2014 when HOM precursors and NO were present at relatively high levels. They also showed that NO_3-radical-initiated autoxidation may contribute to HOMs at night. The weekly concentrations of $C_{7\text{-}10}$ RO_2 radicals ranged from 1×10^5 to 1×10^7 cm^{-3}. Although 17 radicals were identified and classified into this group, the

https://doi.org/10.5194/egusphere-2026-2773
Preprint. Discussion started: 15 July 2026

majority of the signal were contributed by $C_{10}H_{15}O_{6,8,10}$, which are typical monoterpene-derived radicals initiated by O_3. For the subgroups of larger molecules, $C_{17\text{-}20}H_yO_z$ weekly concentrations ranged from 1×10^5 to 5×10^6 cm^{-3}, higher than those of $C_{17\text{-}20}H_yO_zN_{1\text{-}2}$, which ranged from 1×10^5 to 1×10^6 cm^{-3}. The largest difference was observed in summer, when $C_{17\text{-}20}H_yO_z$ increased with temperature, whereas $C_{17\text{-}20}H_yO_zN$ remained nearly flat. This is likely due to the low NO_x regime (Fig. 3d), and presumably low NO_3 concentration, in summer limiting the formation of large $C_{17\text{-}20}H_yO_zN_{1\text{-}2}$. The Other $C_{<20}H_yO_z(N)$ group is primarily composed of isoprene- and sesquiterpene-derived HOM monomers. This is clearly supported by a large fraction of the molecules in this group containing 5 or 11-15 carbon atoms. (Fig S3). In contrast, the Other $C_{\geq 20}H_yO_z(N)$ group comprises high-molecular-weight compounds, typically ranging from 500 to 700 Th. As illustrated in Fig S3, the majority of these species possess carbon numbers of 21, 24, 25, 29, and 30, suggesting they likely originate from the oxidation of larger terpenes (e.g. sesquiterpenes and diterpenes) than monoterpenes (Fig S3). The distribution of oxygen content is presented in Fig S4. The $C_{7\text{-}10}H_yO_z$, $C_{7\text{-}10}$ RO_2, $C_{7\text{-}10}H_yO_zN_{1\text{-}2}$ and Other $C_{<20}H_yO_zN$ groups are characterized by relatively lower oxygen numbers (mostly below 10). In contrast, molecules within the $C_{17\text{-}20}H_yO_z$, $C_{17\text{-}20}H_yO_zN_{1\text{-}2}$ and Other $C_{\geq 20}H_yO_z(N)$ groups exhibit markedly higher oxygen numbers, even though their overall carbon oxidation state is lower due to their larger carbon skeletons. Among these, $C_{17\text{-}20}H_yO_zN_{1\text{-}2}$ appears a bit more highly oxidized than the other two. This is likely because the NO_3 radical is generally required to initiate the autoxidation processes that form $C_{17\text{-}20}H_yO_zN_{1\text{-}2}$ HOMs, and NO_3-initiated first-generation alkyl radicals begin the sequence with three oxygen atoms. In comparison, ignition by O_3 contributes two oxygen atoms, while initiation by the OH radical contributes one or zero, depending on whether the initial reaction proceeds via OH addition or hydrogen abstraction. Another interesting pattern is that in the $C_{17\text{-}20}H_yO_z$ subgroup there is a larger fraction of molecules with fewer than 10 oxygen atoms. The reason could be that molecules within the $C_{17\text{-}20}H_yO_z$ group might not be solely formed from MT RO_2 cross-reaction, but also from the autoxidation of diterpenes, which are supposed to contain fewer oxygen atoms. Further research is required to investigate the impact of this group, particularly given its concentration is comparable to that of the $C_{17\text{-}20}H_yO_z$ and $C_{17\text{-}20}H_yO_zN$ groups.

With this multi-year dataset, we were also able to examine how forest management activities influence the boreal forest atmosphere. A forest thinning activity conducted at the end of March 2020 induced a stress response in the trees, resulting in a drastic increase in both monoterpene and HOM concentrations (Fig. 1 and Fig. S5). Interestingly, CHO HOM subgroups responded much more strongly to thinning than CHON HOM subgroups. This further highlights the limited NO levels in Hyytiälä and their constraining effect on CHON HOM formation.

https://doi.org/10.5194/egusphere-2026-2773
Preprint. Discussion started: 15 July 2026

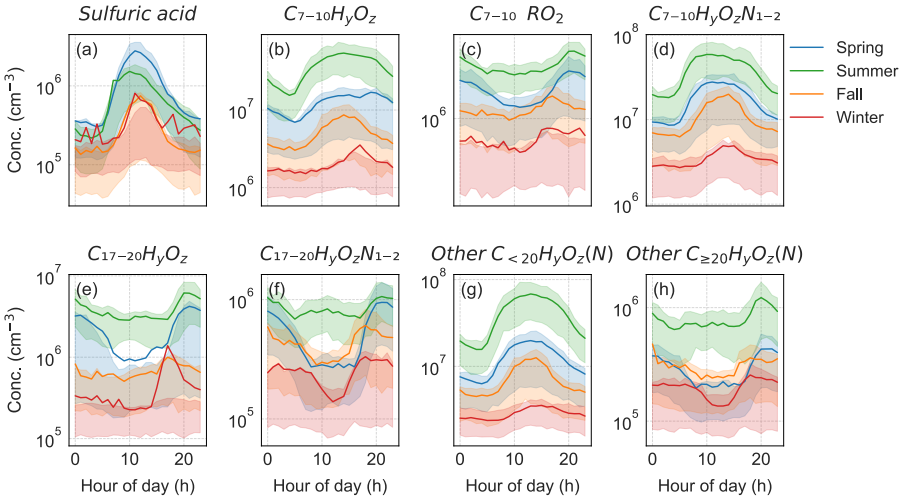

Figure 2: Diurnal variation of (a) Sulfuric acid; (b) $C_{7\text{-}10}H_yO_z$; (c) $C_{7\text{-}10}$ Radicals; (d) $C_{7\text{-}10}H_yO_zN_{1\text{-}2}$; (e) $C_{17\text{-}20}H_yO_z$; (f) $C_{17\text{-}20}H_yO_zN_{1\text{-}2}$; (g) Other $C_{<20}H_yO_z(N)$; (h) Other $C_{\geq20}H_yO_z$ (N) across different season. Line colors indicate seasons, and shaded area represent the 25th-75th percentiles. The season is defined as follows: spring (Mar.-May), summer (Jun.-Aug.), fall (Sep.-Nov.) and Winter (Dec.–Feb.).

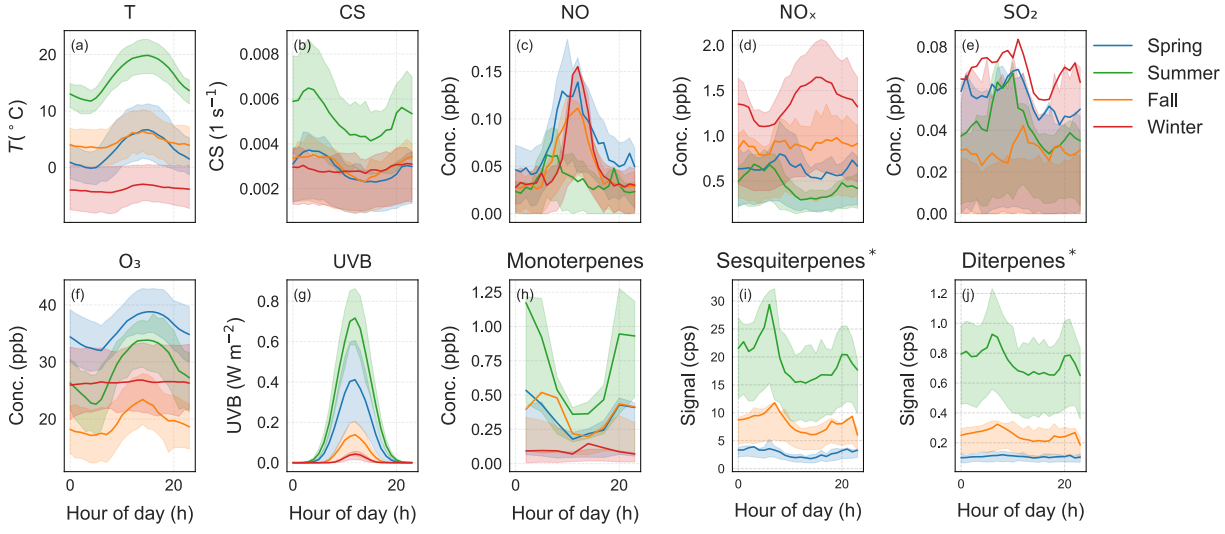

Figure 3: Diurnal variation of (a) Temperature; (b) Condensation sink (CS); (c) Nitrogen monoxide (NO); (d) Nitrogen Oxides (NO_x); (e) Sulphur dioxide (SO_2); (f) Ozone (O_3); (g) Ultraviolet B radiation (UVB); (h) Monoterpenes; (i) Sesquiterpenes; (j) Diterpenes across different seasons. The line colors indicate seasons, and shaded area represent 25th-75th percentiles. The season is defined as follows: spring (Mar.-May), summer (Jun. – Aug.), fall (Sep.- Nov.) and Winter (Dec. – Feb.). *: the seasonal variation of sesquiterpenes and diterpenes is based on a short dataset covering Apr.2022 – Nov. 2022 due to availability.

Figures 2 and 3 present the diurnal variations of low-volatility vapors and related environmental variables across seasons. SA concentrations reach their maximum in spring and summer, whereas HOMs peak predominantly during summer. These

https://doi.org/10.5194/egusphere-2026-2773
Preprint. Discussion started: 15 July 2026

seasonal patterns are attributed to favorable precursor availability and environmental conditions, such as enhanced UVB radiation, higher temperatures, and elevated concentrations of BVOCs including monoterpenes, sesquiterpenes and diterpenes during the warm season (Figs. 3a, h-j). The condensation sink (CS) is also higher in summer and lower in winter, mirroring the seasonal variation of HOMs (Fig. 3b). SA concentrations are elevated during spring and summer, likely driven by the combination of high SO_2 levels and intense UVB radiation during these seasons. The $C_{7\text{-}10}$ radicals, $C_{17\text{-}20}H_yO_z$, and $C_{17\text{-}20}H_yO_zN_{1\text{-}2}$ species exhibit similar diurnal variations, largely tracking the concentration of monoterpenes which peak during the night due to a shallower boundary layer. The $C_{17\text{-}20}$ dimer species also peak at night since during the day the $C_{7\text{-}10}$ RO_2 radicals have many more reaction partners, such as NO and various smaller RO_2 radicals from OH-initiated oxidation of smaller VOC. For these same reasons, $C_{7\text{-}10}H_yO_zN$ and $C_{7\text{-}10}H_yO_z$ peak during the day, due to RO_2 termination by NO, HO_2, or reactions with small RO_2 radicals where dimer formation is less likely (Daub et al., 2024), thus often forming monomeric products even if the reaction is an RO_2 cross reaction.

https://doi.org/10.5194/egusphere-2026-2773
Preprint. Discussion started: 15 July 2026

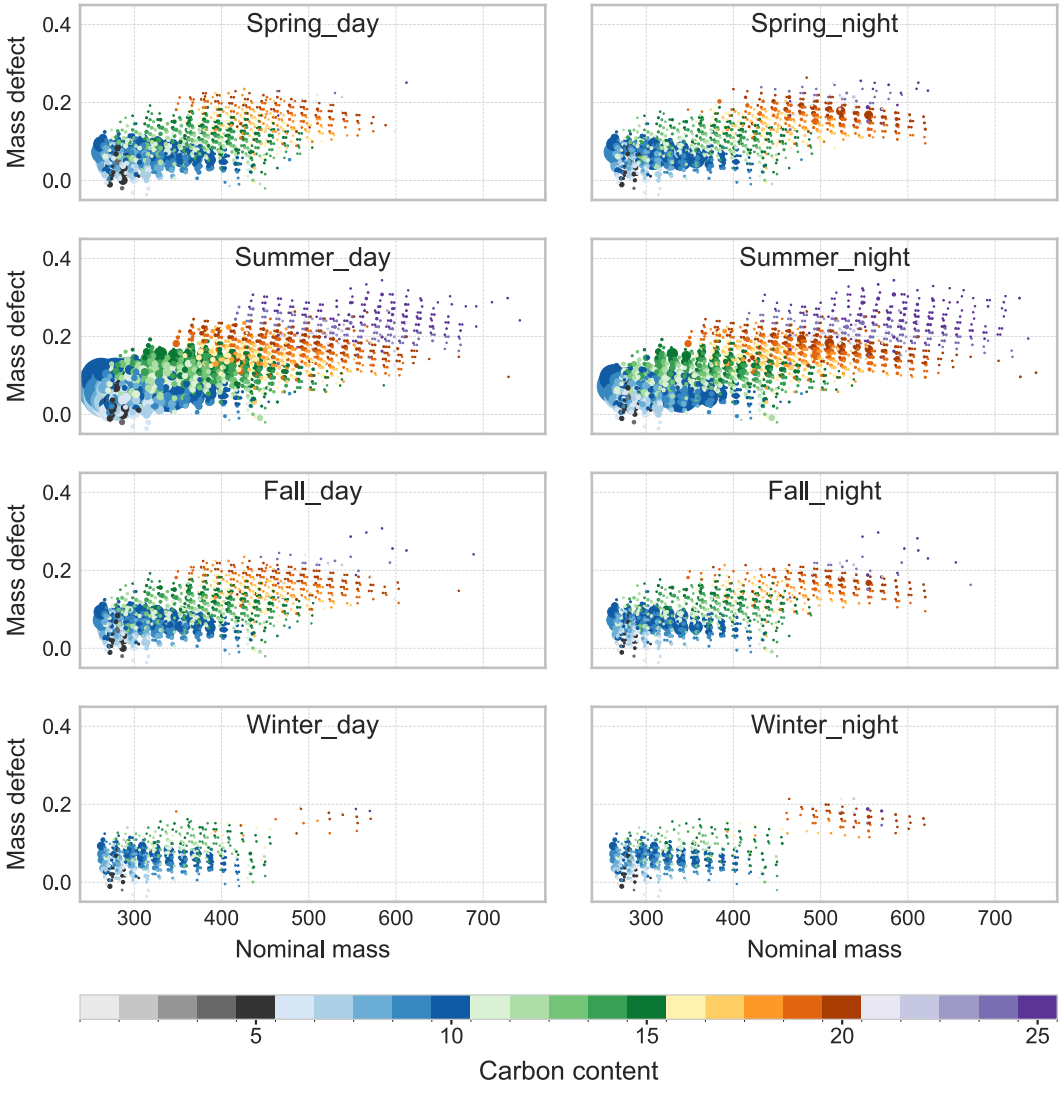

Figure 4: Average daytime and nighttime mass defect plot across seasons (NO_3^- ionization). Daytime and nighttime periods were defined as 10:00–14:00 and 22:00–02:00 (UTC+2), respectively. Dots areas are linearly proportional to the concentration of species. The colors indicate the carbon numbers of each species. Only species with a median concentration above 3500 molecules cm^{-3} are shown (A sensitivity test with a threshold of 1000 and 10000 cm^{-3} is shown in Fig S6 & S7). $C_{15}H_{26}O_5$ and $C_{17}H_{28}O_6$ are not shown in the plot for better visualization, which will be discussed later in conjunction with Fig 5.

Numerous different HOMs were observed throughout the year, even during the winter when the precursor concentrations are low. The mass defect plots for different seasons are shown in Fig 4. Comparing different seasons, the highest amount and concentration of HOMs are detected in summer and the least are detected during winter, because the dominant precursors at our study site are biogenic VOCs emitted from vegetation—a process driven by temperature and sunlight. The patterns in

https://doi.org/10.5194/egusphere-2026-2773
Preprint. Discussion started: 15 July 2026

spring and fall are similar, while the detected HOM concentrations in spring are a bit higher due to more abundant oxidants (Fig. 3f).

Additionally, every band shares a similar pattern in that the detected compounds extend to higher masses in summer, compared to colder seasons. As shown in the seasonal mass defect plots colored by oxygen atom content (Fig. S8), these extended compounds are highly oxidized. This probably indicates that higher ambient temperatures not only regulate HOM concentrations by enhancing terpene emissions but also elevate the oxygenation level of HOMs by kinetically favoring rapid autoxidation steps.

Looking at specific groups, at night, a distinct red band of compounds is observed centered around m/z 500, corresponding mainly to MT–MT HOM dimers (carbon numbers 19-20) and the $C_{17\text{-}20}H_yO_z$ and $C_{17\text{-}20}H_yO_zN_{1\text{-}2}$ groups mentioned in the previous discussion. Although the concentration of this dimer band is higher in summer and more widely distributed, it is constantly observed throughout the year, suggesting that autoxidation and dimerization remain efficient even during cold seasons. The only exception to this seasonal mass extension is that C_{10} compounds show an almost constant mass range throughout the year, probably because they are mostly formed from the dominant BVOCs, monoterpenes, in the boreal forest. Noticeably, a C_{25} band is only detected in summer and shows a slightly higher concentration at night, indicating the formation of cross-reactions between RO_2 radicals from different terpenes.

The increases in concentrations with temperature across different bands are unequal. For example, the daytime concentration of $C_{13\text{-}15}$ molecules (green) in summer is 5.2 times that of spring, while $C_{8\text{-}10}$ (blue) and $C_{18\text{-}20}$ (red) compounds are 3.8 and 2.0 times their spring levels, respectively. The reason is probably that the precursor concentration of C_{15} compounds (assuming they are sesquiterpene HOM monomers) also increase faster than monoterpenes from cold to warm seasons (Fig. 3i). A steeper temperature-dependent emission profile for sesquiterpenes than monoterpenes is also observed in a sub-arctic wetland in Finland (Hellén et al., 2020), implying their potential for forming HOMs during warm seasons. While tropical forests are the largest atmospheric emitter of sesquiterpenes (Wang et al., 2024b), our results highlight that in boreal forests the contribution from sesquiterpenes should not be overlooked, at least during summer. Furthermore, sesquiterpenes react with OH and O_3 approximately 4 and 140 times faster than monoterpenes, respectively (Atkinson and Arey, 2003). However, since their HOM products possess roughly similar atmospheric lifetimes (governed by condensation), the resulting ratio of HOMs to precursors in the ambient atmosphere could differ significantly between the two groups. Consequently, the low ambient abundance of sesquiterpenes should not be misinterpreted as a lack of importance. The corresponding seasonal mass spectra are provided in Fig. S9.

3.2 Bin-NMF result

Bin-NMF analysis was performed separately for mass spectra in the m/z 260-450 and m/z 450-700 ranges to investigate the different sources or processes contributing to HOM monomers and dimers. We selected a year of data without significant gaps to the analysis. The initial mass ranges were selected based on prior knowledge of typical HOM monomer and dimer peaks

https://doi.org/10.5194/egusphere-2026-2773
Preprint. Discussion started: 15 July 2026

(Ehn et al., 2014; Yan et al., 2016), and subsequently adjusted iteratively to obtain more reasonable and interpretable results. The derived factors were found to be relatively insensitive to the exact choice of mass range. The number of factors in the bin-NMF model was selected based primarily on three criteria: (1) the model results adequately explain the observations; (2) contaminant peaks are mostly separated into individual factor; and (3) the majority of factors are interpretable. Generally, the NMF model performed well, successfully distinguishing factors with clear characteristics and identifying contamination profiles (e.g. water cluster factors). Note that not all factors are fully understood, as will be discussed, but the purpose of applying bin-NMF was to extract chemical information from the complex mass spectrometry data and gain insights, rather than to provide a complete explanation of all measured signal. A comparison between the measurement and the bin-NMF result is provided in Fig S10. In this section, we will present the factorization results for the two mass ranges and the contribution from each factor and then discuss the main formation pathways of HOMs at SMEAR II.

The chemistry governing HOM formation remained relatively consistent during spring, autumn, and winter, whereas distinct features emerged in summer for both smaller and larger molecules, likely driven by changes in precursor availability, NO levels, and temperature. The profiles of all factors are clearly separated, each showing distinct fingerprint peaks. Moreover, all factor profiles display peaks appearing in groups, which is consistent with our expectations and likely indicates reliable model performance. This is because the compounds detected by nitrate ionization, especially in the higher mass range, are predominantly formed through autoxidation, a stepwise O_2-addition process. As a result, compounds originating from the same oxidation process appear in the mass spectra as grouped peaks separated by an interval of 16.

Fig 5 shows the bin-NMF results for the m/z 260-450 range. A seven-factor solution was resolved, comprising two source-related profiles (sawmill and contaminant) alongside five distinct chemical profiles: C_{15}/C_{17} HOMs, MT short-chain CHON HOM monomers, MT short-chain CHO HOM monomers, MT CHON HOM monomers and MT CHO HOM monomers. The fingerprint peaks for these different factors can be found in Table 1. We chose the bin-NMF result with seven factors, out of which two are related to specific sources. Factor 1 can be connected to the wind direction coming from a nearby sawmill, which is known to provide monoterpene-rich air masses to the station (Ylivinkka et al., 2025). This factor has only a few prominent peaks and low spectral complexity, and its intensity is elevated when the air comes from the southeast, where the sawmill is located (Fig. S11). Factor 5 is a contamination factor characterized by water peaks spreading across the spectrum that does not have a clear diurnal pattern.

https://doi.org/10.5194/egusphere-2026-2773
Preprint. Discussion started: 15 July 2026

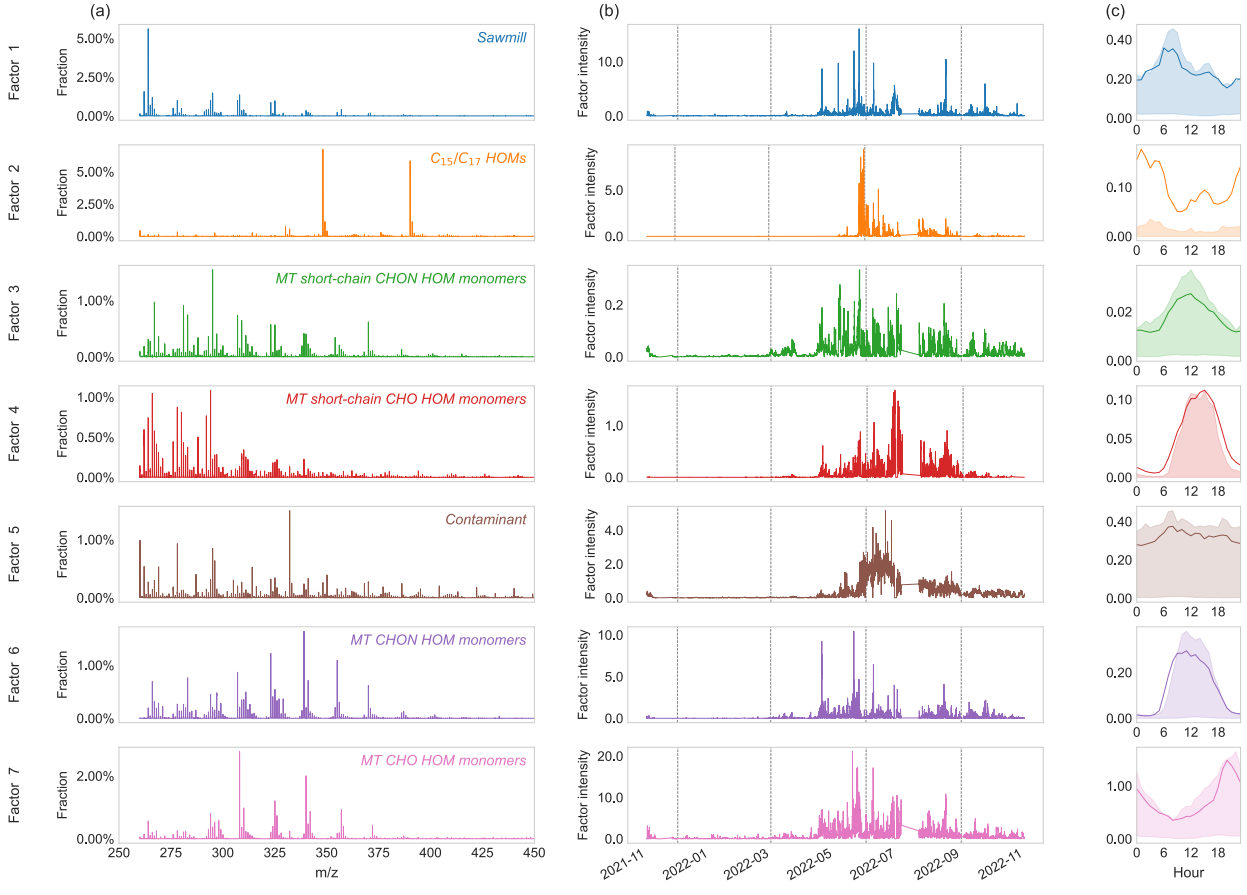

Figure 5: Bin-NMF results for the mass spectrum in the range m/z 260–450. (a) Factor profiles; (b) Time series of factor intensities; (c) Mean diurnal variations of factor intensities. The shaded areas represent the 25th -75th percentiles

Of the remaining five factors, four are connected to HOM monomers but the formation process of Factor 2, remains less certain. It is dominated by two exceptionally high-concentration molecules ($C_{15}H_{26}O_5$&$C_{17}H_{28}O_6$). Although $C_{15}H_{26}O_4$ is also present, its signal is much lower. The factor's time series shows a peak in late May, recurring every year but with varying magnitude (not shown). This recurring feature suggests that the factor is not an instrumental artifact, and the sharp increases in these two dominant peaks can also be observed using the Br^- chemical ionization scheme (not shown). The diurnal pattern, with higher concentrations at night, further hints that this factor could represent isoprene–monoterpene HOM dimers, due to the longer lifetime of RO_2 radicals at night. Factor 6 represents CHON HOM monomers, comprising molecules typically terminated by NO. The compounds in Factor 7 are mostly direct closed-shell products from O_3-initiated RO_2 radicals (e.g. $C_{10}H_{15}O_{8,10}$) and their termination products (Ehn et al., 2014). Fig. S12b further demonstrates that these factors are distinctly separated by their nominal masses according to the nitrogen rule. Specifically, the fingerprint molecules for the nitrate HOM

https://doi.org/10.5194/egusphere-2026-2773
Preprint. Discussion started: 15 July 2026

factor (Factor 6) exhibit odd nominal masses due to the inclusion of a nitrogen atom, whereas the non-nitrate species (Factor 7) display even nominal masses.

Factors 3 and 4 are classified as short-chain MT-derived HOM monomers, with Factor 4 representing CHO species and Factor 3 representing CHON species. This distinction is evident from the factor profiles (Fig 5a) and the mass defect plot of their fingerprint molecules (Fig S12b): Factor 3 exhibits high signals at odd mass numbers, while the dominant peaks in factor 4 appear at even numbers. The few even-numbered bins in Factor 3 represent molecules containing two nitrogen atoms (e.g. $C_5H_{10}N_2O_{7,8}$ and $C_{10}H_{16}N_2O_9$). Apart from some low-signal $C_{4\text{-}6}$ molecules, most of their dominant peaks have a 10-carbon backbone with some fragmentation resulting in loss of one or two carbons. Comparing their diurnal variations, short-chain CHO HOM monomers (Factor 4) reach their maxima later in the day, following the diurnal pattern of atmospheric temperature and O_3, while their CHON counterparts (Factor 3) display a peak at noon, more closely tracking NO. The formation pathways of these short-chain HOM monomers remain unclear, but their correlation with temperature and their smaller molecular sizes may indicate they are likely semi-volatile species. These compounds may partition more into the gas phase during the warm afternoon and then condense more towards the particles when it gets colder. This contrasts with larger HOM species which are unlikely to evaporate once condensed. Previously, Yan et al. (2016) also identified a fragment-like factor at this site, primarily characterized by C_3-C_7 HOM fingerprint molecules.

Table 1: Fingerprint molecules in different factors (m/z 260-450)

Factors	Fingerprint molecules*
1. Sawmill	$C_9H_{14}O_5$, $C_9H_{15}NO_6$, $C_{10}H_{16}O_4$, $C_{20}H_{32}O_7$
2. C_{15}/C_{17} HOMs	$C_{15}H_{26}O_{4,5}$, $C_{17}H_{28}O_6$
3. MT short-chain CHON HOM monomers	$C_4H_6N_2O_{9,10}$, $C_5H_{10}N_2O_{7,8}$, $C_6H_{12}N_2O_7$, $C_6H_9NO_7$, $C_7H_9NO_{6,7}$, $C_8H_{11}NO_7$, $C_7H_{11}NO_{6,7}$, $C_8H_{13}NO_6$, $C_9H_{15}NO_6$, $C_9H_{13}NO_7$, $C_9H_{12}N_2O_9$, $C_{10}H_{14,16}N_2O_9$,
4. MT short-chain CHO HOM monomers	$C_7H_{10}O_7$, $C_8H_{10,12}O_6$, $C_9H_{12,14}O_{5,6}$, $C_{10}H_{16}O_{5,6,7}$, $C_{10}H_{14}O_{5,6}$, $C_{10}H_{18}O_5$, $C_{11}H_{16}O_6$, $C_{12}H_{18}O_{6,7}$
5. Contaminant	Water clusters

https://doi.org/10.5194/egusphere-2026-2773
Preprint. Discussion started: 15 July 2026

6. MT CHON HOM monomers	$C_5H_5NO_9$, $C_5H_7NO_9$, $C_8H_{13}NO_9$, $C_9H_{12}N_2O_{12}$, $C_{10}H_{15,17}NO_{6,7,8,9}$, $C_{10}H_{13}NO_7$, $C_{10}H_{16}N_2O_9$
7. MT CHO HOM monomers	$C_{10}H_{14}O_{6,7,9,11}$, $C_{10}H_{16}O_9$, $C_{10}H_{15}O_{6,8,10}$

*The fingerprint molecules were chosen based on factor profiles in Fig. 5(a) and explained fraction profile in Fig. S12

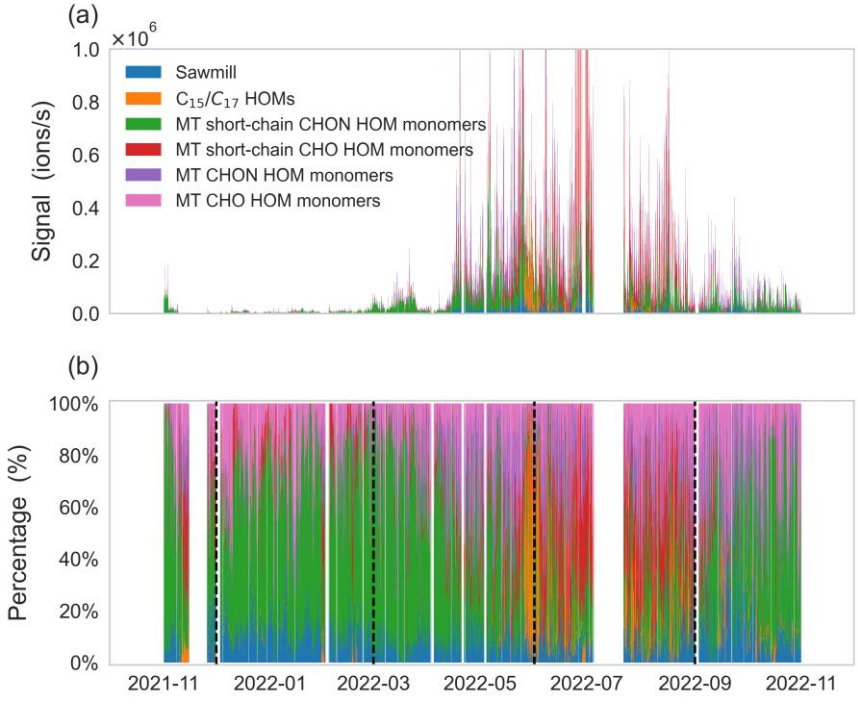

Figure 6: (a) Temporal variation of factor contributions (signal); (b) Temporal variation of factor contributions (percentage). The contaminant factor is excluded.

The temporal variations of factor contributions and relative percentages are shown in Fig 6. We excluded the contaminant factor from this analysis as it does not contain HOMs. The compositional distribution of HOMs remains relatively consistent in winter, spring and fall (Fig 6b). However, during the transition from spring to summer (April to May), the signals of all four MT-related HOMs start to increase, and the MT short-chain CHO HOM monomers dominate the total HOM concentration in summer. The C_{15}/C_{17} HOMs factor shows a strong burst in late May (26^{th}-31^{st}) but disappears rapidly afterward. Starting from September, the distribution gradually returns to the pattern observed in winter and early spring.

https://doi.org/10.5194/egusphere-2026-2773
Preprint. Discussion started: 15 July 2026

The MT short-chain CHON HOM monomers accounted for more than 50% of the signal in the m/z 260-450 range in all seasons except summer. This is likely due to the relatively low NO concentrations in summer compared to other seasons (Fig. 3c). Consequently, the short-chain CHON HOM monomers are replaced by their CHO counterparts. If we combine these two short-chain factors, they constantly account for approximately 70% of the signals of detected molecules in the m/z 260-450 range throughout the year (except for the short spring-to-summer transition), regardless of substantial environmental changes. For example, this stability persists despite snow cover in winter and large temperature variation (-20ºC to 20ºC). The observed high concentrations of short-chain HOMs might be related to their lower loss rate through condensation due to their higher volatility.

Note that the daytime NO concentration averages only about 100 ppt in most seasons, dropping further in summer. The shift from CHON to CHO HOMs clearly demonstrates how efficiently and rapidly low levels of NO can affect the fate of RO_2 and reshape the HOM compositional distribution. With rising temperatures and decreasing NO_x concentrations due to global warming and air pollution control, the summertime characteristics of HOM composition may gradually extend into spring and autumn.

https://doi.org/10.5194/egusphere-2026-2773
Preprint. Discussion started: 15 July 2026

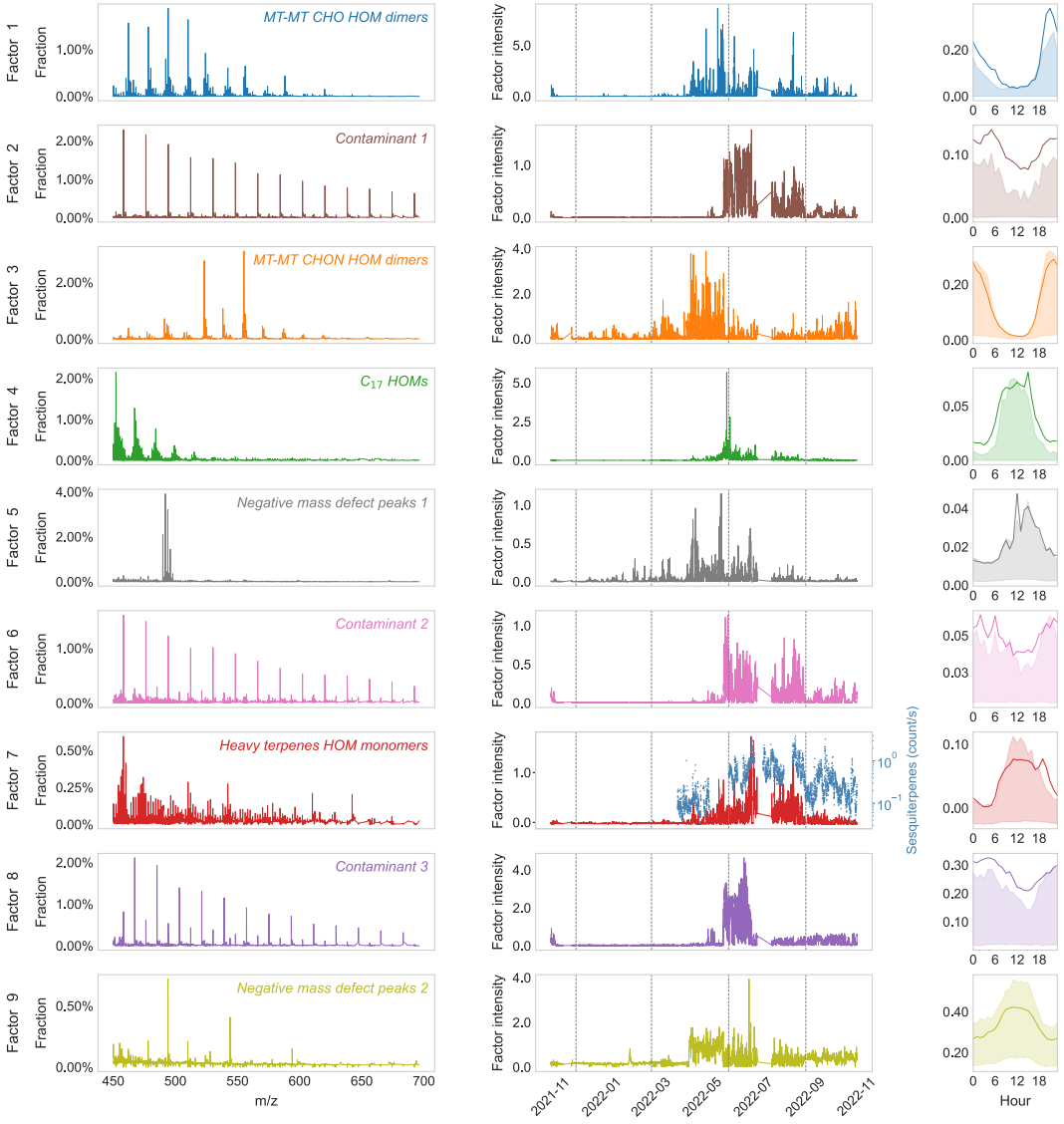

Figure 7: Bin-NMF results of mass spectrum in a range of m/z 450-700. (a) Factor profiles in factors; (b) Time series of factor intensities; (c) Diurnal variations of factor intensities. A baseline removal method was applied to factor 7.

435

A nine-factor solution was selected for the bin-NMF analysis in the m/z 450-700 range (Fig. 7). Among the nine factors, Factors 2, 6, and 8 represent water cluster factors. Factors 2 and 6 are dominated by $(H_2O)_{22\text{-}35}(NO_3)^-$, whereas the dominant peaks in Factor 8 are $(H_2O)_{19\text{-}31}(HNO_3)NO_3^-$. Factor 9 is likely attributed to fluorinated species artificially introduced from the instrument setup, as its dominant peaks exhibit a mass interval of 50 Th (CF_2). Yin et al. (2025) recently reported a similar
440 fluorinated contaminant factor in bin-PMF analyses of nitrate-CIMS data, attributing its origin to the Teflon tubing used in the sampling system. Factors 2, 6, 8 and 9 are classified as contamination factors also due to their abnormal time series and highly

https://doi.org/10.5194/egusphere-2026-2773
Preprint. Discussion started: 15 July 2026

regular signal profiles. In addition, the dominant peaks in Factor 5 are several unassigned negative-mass-defect peaks. We consider all of these to be contamination factors and exclude them from further discussion, although we cannot entirely rule out the possibility that these peaks correspond to real atmospheric molecules.

Factors 1 and 3 correspond to MT-MT CHO HOM dimers and MT-MT CHON HOM dimers, exhibiting the characteristic peaks previously observed in Hyytiälä (Ehn et al., 2014; Yan et al., 2016). The MT–MT CHO HOM dimers show diurnal variations and time series very similar to those of MT CHO HOM monomers and radicals (Fig. 5c and Fig. S14), supporting the assignment that they are mainly formed from RO_2 self- and cross- reactions. Factor 4 comprises several groups of C_{16} and C_{17} molecules with a sequentially increasing number of oxygen atoms. Its time series show an overlapping burst period with the C_{15} and C_{17} factors identified from the bin-NMF results for small molecules (m/z 260–450) (Fig. 5b and Fig. S15). The daytime peak in its diurnal variation suggests that these are likely HOM monomers; however, we are not aware of BVOC precursors in the boreal forest having a carbon number of 17. Alternatively, these peaks may represent fragmentation products. Factor 7 corresponds to HOM monomers derived from heavy terpenes (sesquiterpenes and diterpenes). The dominant peaks are $C_{15}H_{24,26}O_{9\text{-}12}$ and additional C_{20} molecules observable at higher masses within this profile. The time series of this factor's signal follows that of the sesquiterpene signal in both spring and summer. The discrepancy observed in autumn is likely due to insufficient oxidants, such as O_3 (Fig. 3f). Coupled with a daytime peak in its diurnal variation, these observations indicate that Factor 7 represents heavy terpene-derived HOM monomers. The fingerprint molecules for the different factors in the m/z 450-700 range can be found in Table 2.

Table 2: Fingerprint molecules in different factors (m/z 450-700)

Factors	Fingerprint molecules*
1: MT-MT CHO HOM dimers	$C_{19}H_{28}O_{9,11,13}$, $C_{20}H_{32}O_{9,11,13,14,15}$, $C_{19}H_{30}O_{10,12}$, $C_{20}H_{30}O_{10,16}$
2: Contaminant 1	$(H_2O)_{22\text{-}35}NO_3^-$
3: MT-MT CHON HOM dimers	$C_{20}H_{31}NO_{9,11,13}$
4: C_{17} HOMs	$C_{17}H_{28}O_{7,9}$, $C_{17}H_{26}O_{8,9,10,11,13}$, $C_{16}H_{25}NO_{10,11}$, $C_{17}H_{27}NO_{9,10,12,13}$
5: Negative mass defect peaks 1	m/z 489.87, 491.87, 493.86, 495.86
6: Contaminant 2	$(H_2O)_{22\text{-}35}NO_3^-$

https://doi.org/10.5194/egusphere-2026-2773
Preprint. Discussion started: 15 July 2026

7: Heavy terpenes HOM monomers	$C_{15}H_{24}O_{9,10,11,12}$, $C_{15}H_{26}O_{9,10,11,12}$, $C_{20}H_{30}O_{10}$ $C_{20}H_{32}O_{13}$, $C_{19}H_{30}O_{12}$
8. Contaminant 3	$(H_2O)_{19\text{-}31}(HNO_3)NO_3^-$
9: Negative mass defect peaks 2	m/z 494.99, 543.98, 593.98

***The fingerprint molecules were chosen based on factor profiles in Fig. 7(a) and explained fraction in Fig. S13**

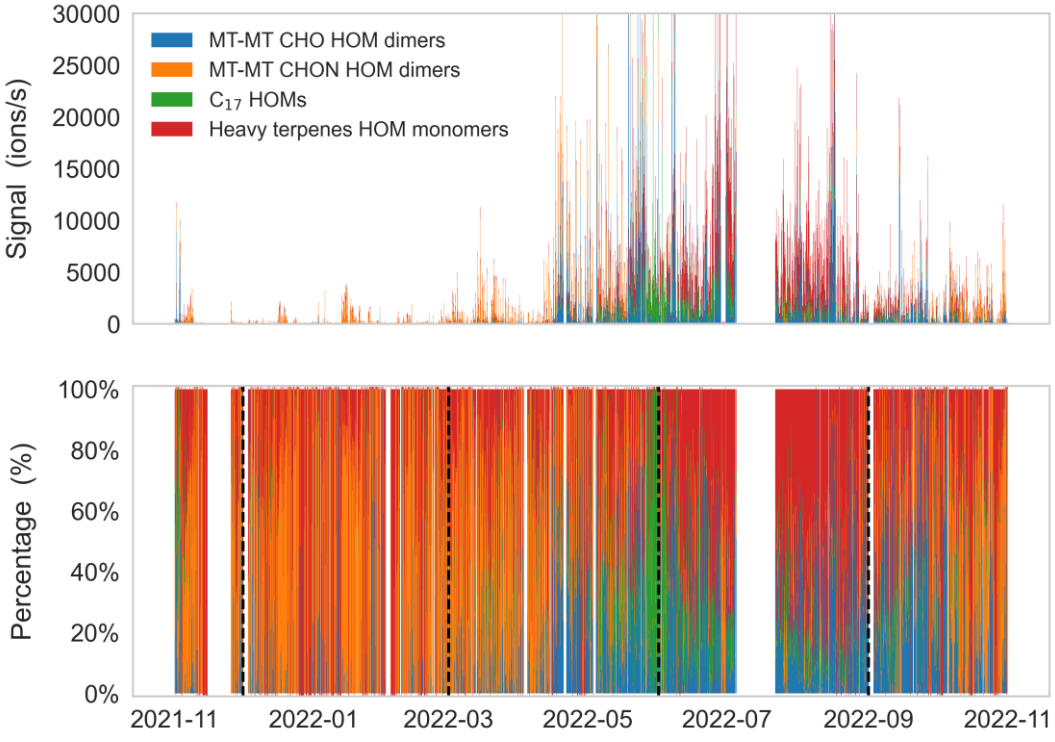

Figure 8: (a) Temporal variation of source contributions (signal); (b) Temporal variation of source contributions (percentage). Three contaminant factors and two negative mass defect peaks factors are excluded. A baseline removal method was applied to factor 7.

The signal in the m/z 450-700 range is quite low during winter, and the few elevated episodes observed at night are mainly driven by MT-MT CHON HOM dimers (Fig. 8). In spring there is a transition period when temperatures increase rapidly, and NO levels decrease. As a result, MT–MT CHON HOM dimers first dominate the total signal in early spring, whereas MT–MT CHO dimers start to influence the signal in late spring. Subsequently, the C_{17} HOM factor appears briefly for several days before disappearing, after which heavy terpene-derived HOM monomers dominate the signals throughout the rest of the summer. The heavy terpene factor accounts for 50 - 80% of the signal during the daytime in summer, indicating that heavy

https://doi.org/10.5194/egusphere-2026-2773
Preprint. Discussion started: 15 July 2026

475 terpenes, mainly sesquiterpenes, are important for HOMs formation and potentially initial growth of newly formed particles. Autumn mirrors the transitional trend observed in spring but in the opposite direction, gradually reverting to the winter and early spring pattern.

3.3 Volatility

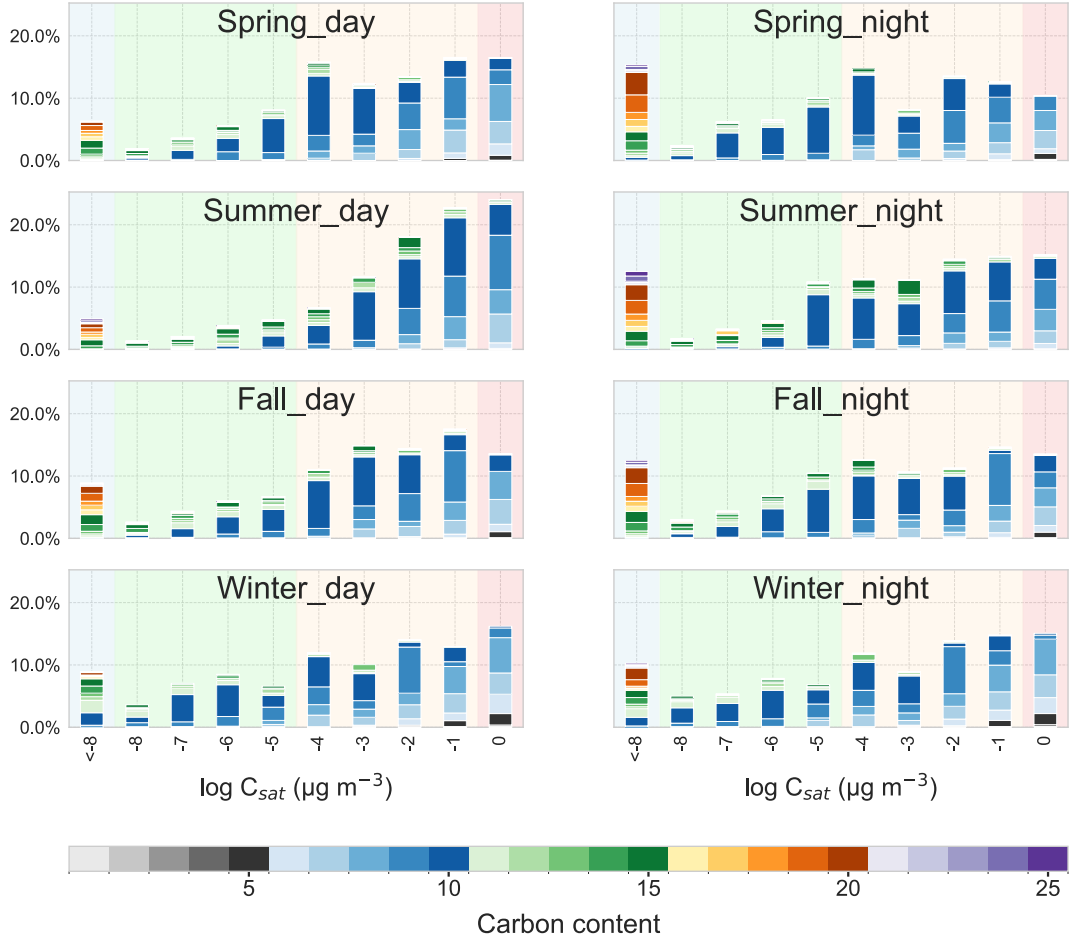

480

Figure 9: Volatility distribution of HOMs across seasons divided to daytime and nighttime. The bar colors indicate carbon numbers. Daytime and nighttime periods were defined as 10:00–14:00 and 22:00–02:00 (+1) (UTC+2), respectively. Only molecules with a logC_{sat} lower than 1 μg m^{-3} are shown. The pink area is semi-volatile compounds, faint yellow is low volatile compounds, green is extremely low volatile compounds, and blue is ultra-low volatile compounds. The volatility is estimated by a
485 **parameterization from (Mohr et al., 2019), using average temperatures during day and night in different seasons. Only molecules with a median concentration above 3500 molecules m^{-3} are shown in this plot.**

Volatility is a key property that determines the atmospheric behavior of molecules, such as their ability to condense onto surfaces and participate in particle formation. Semi-volatile compounds are relatively more volatile and can potentially

https://doi.org/10.5194/egusphere-2026-2773
Preprint. Discussion started: 15 July 2026

evaporate from particles. In contrast, low- to ultra-low-volatility molecules are generally considered to irreversibly condense onto particle surfaces. In this section, we will first show the seasonal variation of the HOM volatility distribution and then discuss the link between HOM species and their volatility classes, along with their subsequent potential impact on new particle formation and growth. Volatility was estimated using the parameterization developed by Mohr et al. (2019), incorporating average daytime and nighttime temperatures across different seasons. We selected this widely used method to facilitate comparisons with existing literature (Graham et al., 2023; Yan et al., 2021); however, the inherent uncertainties of this parameterization must be acknowledged. For instance, Peräkylä et al. (2020) found that this approach tends to yield lower volatility estimates for α-pinene-derived CHO HOM monomers compared to alternative methods.

In Fig S16, we compare the concentration of measured molecules across volatility bins and seasons. Overall, the HOM concentrations in each bin exhibit a similar seasonal trend, with higher values in the warm season and lower values in the cold season. The diurnal variation in concentration is relatively small compared to the observed seasonal variation. When comparing daytime median concentrations, LVOCs show the most pronounced seasonal decrease, falling by a factor of 17.3 from summer to winter. In comparison, ULVOCs and ELVOCs decrease by a factor of 8.2 and 6.7, respectively. Crucially, the non-uniform increase in the concentrations of different volatility classes indicates that an increase in total HOM concentration does not directly translate to an enhanced capacity for nucleation. During the night, seasonal variations are more uniform across the three volatility classes: ULVOC concentrations decrease by a factor of 9.6, ELVOCs by 6.2, and LVOCs by 7.9.

Fig 9 shows the relative contribution of each volatility class to HOMs color-coded by carbon atom number. During the daytime, the HOM volatility distribution shifts towards the more volatile range in summer, characterized by a steep upward gradient from low to relatively higher volatility bins. In contrast, the winter distribution is significantly flatter. This highlights the dominant role of temperature in shaping HOM distributions. This effect is further evidenced by specific compounds, such as C_{15} species, which spread from the ULVOC to LVOC range during summer, whereas they predominantly reside in the ULVOC and ELVOC fractions during cooler seasons. Interestingly, the nocturnal volatility distribution exhibits minimal seasonal variation, despite mean temperatures ranging from -6.0 °C in winter to 13.8 °C in summer.

Regarding molecular composition, C_{20} compounds are the main contributors to ULVOCs year-round except in winter. Their contribution is particularly pronounced at night, likely because C_{15} compounds lack efficient nocturnal production pathways, whereas C_{20} compounds can be formed via nighttime dimerization. The volatility of C_{15} compounds shifts significantly due to drastic seasonal temperature changes; they span the ULVOC-to-LVOC range during summer but are confined mainly to the ULVOC fraction during winter days. This suggests that sesquiterpenes might play a much more important role in new particle formation and growth in the boreal forest than previously thought, as they account for approximately 50% of the total ULVOC concentration in spring -- the season with highest NPF frequency (Vana et al., 2016). The contribution of C_{15} compounds to ULVOCs remains similar from spring to summer, despite C_{15} compounds showing the most drastic increase in concentration. This is likely due to the high temperatures in summer shifting the volatility of C_{15} compounds towards more volatile ranges. C_{10} compounds remain the primary contributors to the LVOC and ELVOC fractions, except during summer days when high temperatures restrict them to the LVOC and SVOC ranges. Certain C_{11} compounds ($C_{11}H_{16}O_{8\text{-}10}$), mainly classified as

https://doi.org/10.5194/egusphere-2026-2773
Preprint. Discussion started: 15 July 2026

ELVOCs, are present constantly throughout the year. These species constitute a larger proportion of the ULVOCs and ELVOCs in winter when sesquiterpene concentrations are low, although their formation pathway remains unclear. Fig S17 illustrates a seasonal decrease in the CHON fraction from cooler to warm season, driven by reduced NO availability. This reduction is observed consistently across every volatility class.

4 Conclusions

In this study, we present, to the best of our knowledge, the longest continuous atmospheric observations (nearly four years) of low-volatility vapors—specifically sulfuric acid and Highly Oxygenated Organic Molecules (HOMs) — measured via NO_3^--CIMS in a boreal forest. By applying high-resolution peak fitting to assign ~1400 peaks and utilizing a bin-NMF method, we extracted key chemical information to deconvolve this massive, complex dataset. Our results show that total HOM concentrations are primarily regulated by temperature-dependent terpene emissions across seasons. We observe distinct diurnal patterns: HOM monomers peak during the day due to the availability of oxidants and precursors, while dimers peak at night, driven by extended RO_2 radical lifetimes under low concentrations of terminating species (NO and HO_2). Furthermore, our bin-NMF results reveal that HOM formation pathways at SMEAR II are strongly modulated by seasonality. During colder months, monoterpene-derived CHON HOMs dominate the spectrum. In contrast, summertime chemistry—characterized by lower NO concentrations (<100 ppt) that limit the NO termination pathway of RO_2 radicals—shifts toward CHO species and a substantial contribution from heavy terpenes (sesquiterpenes and diterpenes), which account for 40–80% of the signal in the high-mass range (m/z 450–700).

Compared to previous short-term studies, we emphasize the pronounced seasonal variations in HOM concentration and molecular composition. We demonstrate that these distinct seasonal dynamics are a combined result of changing terpenes emissions and shifting formation mechanism under different environmental conditions. Notably, while C_{10} HOMs remain the primary contributors to the total HOM concentration, we found that C_{15} compounds exhibit the most rapid seasonal increase during summer and contribute significantly to the daytime ULVOC budget across all seasons. This finding challenges the previously held assumption that monoterpenes are the only critical BVOCs for HOM formation in boreal forests (Ehn et al., 2014; Jokinen et al., 2022b).

Despite the robustness of this long-term dataset, several caveats must be considered. Quantifying HOMs requires the assumption that all molecules are charged at the kinetic limit, which yield a lower-limit estimation of HOM concentration. Moreover, the limited number of calibrations and the lack of transmission efficiency calibration introduce additional uncertainties. While these caveats affect absolute quantification, they do not impact the robustness of the observed seasonal trends.

While warmer summer temperatures increase total HOM concentrations, they concurrently shift the volatility distribution toward higher volatility classes (LVOCs/SVOCs). Despite this shift, our data show that sesquiterpene-derived $C_{13\text{-}15}$ HOMs and $C_{17\text{-}20}$ HOMs contribute comparably to the daytime ULVOC budget year-round. Critically, during the spring maximum of

https://doi.org/10.5194/egusphere-2026-2773
Preprint. Discussion started: 15 July 2026

new particle formation (NPF) events, C_{13-15} HOMs dominate the daytime ULVOC pool, accounting for approximately 40.6% of the total concentration and exceeding the 28.3% contribution from C_{17-20} HOMs. This underscores the crucial, yet often underestimated, role of sesquiterpene oxidation in driving daytime nucleation. Ultimately, these findings indicate that seasonal BVOC emissions and specific HOM formation mechanisms must be explicitly represented in climate and atmospheric models. By bridging key knowledge gaps regarding the seasonal variation, compositional distribution, and volatility of HOMs, this dataset provides a more accurate framework for assessing long-term atmosphere-forest interactions and their broader climate feedback mechanisms.

Code and data availability

The dataset will be available in Zenodo

Author contributions

CL and NS conceptualized the original idea of this study. CL performed data analysis and wrote the paper under the supervision of NS and ME. LA helped with pre-process of MION-APi-TOF data. IY and PK were responsible for VOC and NO measurement. All authors contributed to the discussion of results and provided input for the paper.

Competing interests

At least one of the (co-)authors is a member of the editorial board of *Atmospheric Chemistry and Physics*.

Disclaimer

Copernicus Publications remains neutral with regard to jurisdictional claims made in the text, published maps, institutional affiliations, or any other geographical representation in this paper. While Copernicus Publications makes every effort to include appropriate place names, the final responsibility lies with the authors. Views expressed in the text are those of the authors and do not necessarily reflect the views of the publisher.

Acknowledgements

The scientific and technical staff of the SMEAR II station, especially Reijo Pilkottu, Matti Loponen and Sirpa Rantanen, are acknowledged for their weekly work towards good quality data. Jyri Mikkilä, Oskari Kausiala and Jani Hakala and Karsa are acknowledged for their help with starting the first field measurements with MION-inlet. Colleagues at INAR are acknowledged

https://doi.org/10.5194/egusphere-2026-2773
Preprint. Discussion started: 15 July 2026

for help in conducting the measurements. Petri Keronen is acknowledged for the NO_x measurements. The station is part of the European research infrastructure ACTRIS (Aerosol, Clouds and Trace Gases Research Infrastructure). ACTRIS CiGas – Centre for Reactive Trace Gases In Situ Measurements is acknowledged for providing operation support to the reactive trace gases instruments at the station.

The authors acknowledge the use of AI for language editing and proofreading purposes.

Financial support

The Research Council of Finland research infrastructure projects are acknowledged (INAR RI/ ACTRIS-FI 2020-2024 grant no. 328616, INAR RI 2022-2025 grant no. 345510 and INAR RI 2024-2027 grant no. 358647). The ACCC (Atmosphere and Climate Competence Center) Flagship funding by the Research Council of Finland (grant no. 337549, 357902, 359340) and Jane and Aatos Erkko Foundation funding are acknowledged. EU funding supporting ACTRIS activities and implementation are also acknowledged: ACTRIS IMP (grant no. 871115), ATMO-ACCESS (grant no. 101008004) and RI-URBANS (grant no. 101036245).

References

Atkinson, R. and Arey, J.: Atmospheric Degradation of Volatile Organic Compounds, Chem. Rev., 103, 4605–4638, https://doi.org/10.1021/cr0206420, 2003.

Baker, Y., Kang, S., Wang, H., Wu, R., Xu, J., Zanders, A., He, Q., Hohaus, T., Ziehm, T., Geretti, V., Bannan, T. J., O'Meara, S. P., Voliotis, A., Hallquist, M., McFiggans, G., Zorn, S. R., Wahner, A., and Mentel, T. F.: Impact of HO_2/RO_2 ratio on highly oxygenated α-pinene photooxidation products and secondary organic aerosol formation potential, Atmospheric Chem. Phys., 24, 4789–4807, https://doi.org/10.5194/acp-24-4789-2024, 2024.

Barreira, L. M. F., Ylisirniö, A., Pullinen, I., Buchholz, A., Li, Z., Lipp, H., Junninen, H., Hõrrak, U., Noe, S. M., Krasnova, A., Krasnov, D., Kask, K., Talts, E., Niinemets, Ü., Ruiz-Jimenez, J., and Schobesberger, S.: The importance of sesquiterpene oxidation products for secondary organic aerosol formation in a springtime hemiboreal forest, Atmospheric Chem. Phys., 21, 11781–11800, https://doi.org/10.5194/acp-21-11781-2021, 2021.

Bianchi, F., Kurtén, T., Riva, M., Mohr, C., Rissanen, M. P., Roldin, P., Berndt, T., Crounse, J. D., Wennberg, P. O., Mentel, T. F., Wildt, J., Junninen, H., Jokinen, T., Kulmala, M., Worsnop, D. R., Thornton, J. A., Donahue, N., Kjaergaard, H. G., and Ehn, M.: Highly Oxygenated Organic Molecules (HOM) from Gas-Phase Autoxidation Involving Peroxy Radicals: A Key Contributor to Atmospheric Aerosol, Chem. Rev., 119, 3472–3509, https://doi.org/10.1021/acs.chemrev.8b00395, 2019.

Crounse, J. D., Nielsen, L. B., Jørgensen, S., Kjaergaard, H. G., and Wennberg, P. O.: Autoxidation of Organic Compounds in the Atmosphere, J. Phys. Chem. Lett., 4, 3513–3520, https://doi.org/10.1021/jz4019207, 2013.

Curtius, J., Heinritzi, M., Beck, L. J., Pöhlker, M. L., Tripathi, N., Krumm, B. E., Holzbeck, P., Nussbaumer, C. M., Hernández Pardo, L., Klimach, T., Barmpounis, K., Andersen, S. T., Bardakov, R., Bohn, B., Cecchini, M. A., Chaboureau, J.-P., Dauhut, T., Dienhart, D., Dörich, R., Edtbauer, A., Giez, A., Hartmann, A., Holanda, B. A., Joppe, P., Kaiser, K., Keber, T., Klebach, H., Krüger, O. O., Kürten, A., Mallaun, C., Marno, D., Martinez, M., Monteiro, C., Nelson, C., Ort, L., Raj, S. S., Richter, S.,

https://doi.org/10.5194/egusphere-2026-2773
Preprint. Discussion started: 15 July 2026

Ringsdorf, A., Rocha, F., Simon, M., Sreekumar, S., Tsokankunku, A., Unfer, G. R., Valenti, I. D., Wang, N., Zahn, A., Zauner-Wieczorek, M., Albrecht, R. I., Andreae, M. O., Artaxo, P., Crowley, J. N., Fischer, H., Harder, H., Herdies, D. L., Machado, L. A. T., Pöhlker, C., Pöschl, U., Possner, A., Pozzer, A., Schneider, J., Williams, J., and Lelieveld, J.: Isoprene nitrates drive new particle formation in Amazon's upper troposphere, Nature, 636, 124–130, https://doi.org/10.1038/s41586-024-08192-4, 2024.

Dada, L., Stolzenburg, D., Simon, M., Fischer, L., Heinritzi, M., Wang, M., Xiao, M., Vogel, A. L., Ahonen, L., Amorim, A., Baalbaki, R., Baccarini, A., Baltensperger, U., Bianchi, F., Daellenbach, K. R., DeVivo, J., Dias, A., Dommen, J., Duplissy, J., Finkenzeller, H., Hansel, A., He, X.-C., Hofbauer, V., Hoyle, C. R., Kangasluoma, J., Kim, C., Kürten, A., Kvashnin, A., Mauldin, R., Makhmutov, V., Marten, R., Mentler, B., Nie, W., Petäjä, T., Quéléver, L. L. J., Saathoff, H., Tauber, C., Tome, A., Molteni, U., Volkamer, R., Wagner, R., Wagner, A. C., Wimmer, D., Winkler, P. M., Yan, C., Zha, Q., Rissanen, M., Gordon, H., Curtius, J., Worsnop, D. R., Lehtipalo, K., Donahue, N. M., Kirkby, J., El Haddad, I., and Kulmala, M.: Role of sesquiterpenes in biogenic new particle formation, Sci Adv, 9, adi5297, https://doi.org/10.1126/sciadv.adi5297, 2023.

Daub, C. D., Skog, R., and Kurtén, T.: Lifetimes of pre-reactive complexes of peroxy radicals revisited: thermostat effects, temperature dependence and highly oxygenated molecules, Environ. Sci. Atmospheres, 4, 732–739, https://doi.org/10.1039/D4EA00037D, 2024.

Ehn, M., Junninen, H., Petäjä, T., Kurtén, T., Kerminen, V.-M., Schobesberger, S., Manninen, H. E., Ortega, I. K., Vehkamäki, H., Kulmala, M., and Worsnop, D. R.: Composition and temporal behavior of ambient ions in the boreal forest, Atmospheric Chem. Phys., 10, 8513–8530, https://doi.org/10.5194/acp-10-8513-2010, 2010.

Ehn, M., Kleist, E., Junninen, H., Petäjä, T., Lönn, G., Schobesberger, S., Dal Maso, M., Trimborn, A., Kulmala, M., Worsnop, D. R., Wahner, A., Wildt, J., and Mentel, T. F.: Gas phase formation of extremely oxidized pinene reaction products in chamber and ambient air, Atmospheric Chem. Phys., 12, 5113–5127, https://doi.org/10.5194/acp-12-5113-2012, 2012.

Ehn, M., Thornton, J. A., Kleist, E., Sipilä, M., Junninen, H., Pullinen, I., Springer, M., Rubach, F., Tillmann, R., Lee, B., Lopez-Hilfiker, F., Andres, S., Acir, I.-H., Rissanen, M., Jokinen, T., Schobesberger, S., Kangasluoma, J., Kontkanen, J., Nieminen, T., Kurtén, T., Nielsen, L. B., Jørgensen, S., Kjaergaard, H. G., Canagaratna, M., Maso, M. D., Berndt, T., Petäjä, T., Wahner, A., Kerminen, V.-M., Kulmala, M., Worsnop, D. R., Wildt, J., and Mentel, T. F.: A large source of low-volatility secondary organic aerosol, Nature, 506, 476–479, https://doi.org/10.1038/nature13032, 2014.

Eisele, F. L. and Tanner, D. J.: Measurement of the gas phase concentration of H2SO4 and methane sulfonic acid and estimates of H2SO4 production and loss in the atmosphere, J. Geophys. Res. Atmospheres, 98, 9001–9010, https://doi.org/10.1029/93JD00031, 1993.

Finkenzeller, H., Mikkilä, J., Righi, C., Juuti, P., Sipilä, M., Rissanen, M., Worsnop, D., Shcherbinin, A., Sarnela, N., and Kangasluoma, J.: Multiphysical description of atmospheric pressure interface chemical ionisation in MION2 and Eisele type inlets, Atmospheric Meas. Tech., 17, 5989–6001, https://doi.org/10.5194/amt-17-5989-2024, 2024.

Frege, C., Ortega, I. K., Rissanen, M. P., Praplan, A. P., Steiner, G., Heinritzi, M., Ahonen, L., Amorim, A., Bernhammer, A.-K., Bianchi, F., Brilke, S., Breitenlechner, M., Dada, L., Dias, A., Duplissy, J., Ehrhart, S., El-Haddad, I., Fischer, L., Fuchs, C., Garmash, O., Gonin, M., Hansel, A., Hoyle, C. R., Jokinen, T., Junninen, H., Kirkby, J., Kürten, A., Lehtipalo, K., Leiminger, M., Mauldin, R. L., Molteni, U., Nichman, L., Petäjä, T., Sarnela, N., Schobesberger, S., Simon, M., Sipilä, M., Stolzenburg, D., Tomé, A., Vogel, A. L., Wagner, A. C., Wagner, R., Xiao, M., Yan, C., Ye, P., Curtius, J., Donahue, N. M., Flagan, R. C., Kulmala, M., Worsnop, D. R., Winkler, P. M., Dommen, J., and Baltensperger, U.: Influence of temperature on the molecular composition of ions and charged clusters during pure biogenic nucleation, Atmospheric Chem. Phys., 18, 65–79, https://doi.org/10.5194/acp-18-65-2018, 2018.

Graham, E. L., Wu, C., Bell, D. M., Bertrand, A., Haslett, S. L., Baltensperger, U., El Haddad, I., Krejci, R., Riipinen, I., and Mohr, C.: Volatility of aerosol particles from NO_3 oxidation of various biogenic organic precursors, Atmospheric Chem. Phys., 23, 7347–7362, https://doi.org/10.5194/acp-23-7347-2023, 2023.

Guo, Y., Yan, C., Liu, Y., Qiao, X., Zheng, F., Zhang, Y., Zhou, Y., Li, C., Fan, X., Lin, Z., Feng, Z., Zhang, Y., Zheng, P., Tian, L., Nie, W., Wang, Z., Huang, D., Daellenbach, K. R., Yao, L., Dada, L., Bianchi, F., Jiang, J., Liu, Y., Kerminen, V.-M., and Kulmala, M.: Seasonal variation in oxygenated organic molecules in urban Beijing and their contribution to secondary organic aerosol, Atmospheric Chem. Phys., 22, 10077–10097, https://doi.org/10.5194/acp-22-10077-2022, 2022.

Hellén, H., Praplan, A. P., Tykkä, T., Ylivinkka, I., Vakkari, V., Bäck, J., Petäjä, T., Kulmala, M., and Hakola, H.: Long-term measurements of volatile organic compounds highlight the importance of sesquiterpenes for the atmospheric chemistry of a boreal forest, Atmospheric Chem. Phys., 18, 13839–13863, https://doi.org/10.5194/acp-18-13839-2018, 2018.

Hellén, H., Schallhart, S., Praplan, A. P., Tykkä, T., Aurela, M., Lohila, A., and Hakola, H.: Sesquiterpenes dominate monoterpenes in northern wetland emissions, Atmospheric Chem. Phys., 20, 7021–7034, https://doi.org/10.5194/acp-20-7021-2020, 2020.

Huang, W., Sarnela, N., Heikkinen, L., Tham, Y. J., Mikkilä, J., Thomas, S. J., Donahue, N. M., Kulmala, M., and Bianchi, F.: Measurement report: Molecular composition and volatility of gaseous organic compounds in a boreal forest – from volatile organic compounds to highly oxygenated organic molecules, Atmospheric Chem. Phys., 21, 8961–8977, https://doi.org/10.5194/acp-21-8961-2021, 2021.

Isaacman-VanWertz, G., Frazier, G., Willison, J., and Faiola, C.: Missing Measurements of Sesquiterpene Ozonolysis Rates and Composition Limit Understanding of Atmospheric Reactivity, Environ. Sci. Technol., 58, 7937–7946, https://doi.org/10.1021/acs.est.3c10348, 2024.

Jokinen, T., Kausiala, O., Garmash, O., Peräkylä, O., Junninen, H., Schobesberger, S., Chao, yan, Sipilä, M., and Rissanen, M.: Production of highly oxidized organic compounds from ozonolysis of beta-caryophyllene : laboratory and field measurements, Boreal Environ. Res., 21, 262–273, https://doi.org/https://doi.org/10.60910/6kxv-uyg2, 2016.

Jokinen, T., Lehtipalo, K., Thakur, R. C., Ylivinkka, I., Neitola, K., Sarnela, N., Laitinen, T., Kulmala, M., Petäjä, T., and Sipilä, M.: Measurement report: Long-term measurements of aerosol precursor concentrations in the Finnish subarctic boreal forest, Atmospheric Chem. Phys., 22, 2237–2254, https://doi.org/10.5194/acp-22-2237-2022, 2022a.

Jokinen, T., Lehtipalo, K., Thakur, R. C., Ylivinkka, I., Neitola, K., Sarnela, N., Laitinen, T., Kulmala, M., Petäjä, T., and Sipilä, M.: Measurement report: Long-term measurements of aerosol precursor concentrations in the Finnish subarctic boreal forest, Atmospheric Chem. Phys., 22, 2237–2254, https://doi.org/10.5194/acp-22-2237-2022, 2022b.

Kang, S., Wildt, J., Pullinen, I., Vereecken, L., Wu, C., Wahner, A., Zorn, S. R., and Mentel, T. F.: Formation of highly oxygenated organic molecules from α-pinene photooxidation: evidence for the importance of highly oxygenated alkoxy radicals, EGUsphere, 1–33, https://doi.org/10.5194/egusphere-2025-2772, 2025.

Kirkby, J., Amorim, A., Baltensperger, U., Carslaw, K. S., Christoudias, T., Curtius, J., Donahue, N. M., Haddad, I. E., Flagan, R. C., Gordon, H., Hansel, A., Harder, H., Junninen, H., Kulmala, M., Kürten, A., Laaksonen, A., Lehtipalo, K., Lelieveld, J., Möhler, O., Riipinen, I., Stratmann, F., Tomé, A., Virtanen, A., Volkamer, R., Winkler, P. M., and Worsnop, D. R.: Atmospheric new particle formation from the CERN CLOUD experiment, Nat. Geo, 16, 948–957, https://doi.org/10.1038/s41561-023-01305-0, 2023.

Kulmala, M.: Importance of New Particle Formation for Climate and Air Quality, ACS EST Air, 2, 710–712, https://doi.org/10.1021/acsestair.5c00095, 2025.

https://doi.org/10.5194/egusphere-2026-2773
Preprint. Discussion started: 15 July 2026

Kulmala, M., Kontkanen, J., Junninen, H., Lehtipalo, K., Manninen, H. E., Nieminen, T., Petäjä, T., Sipilä, M., Schobesberger, S., Rantala, P., Franchin, A., Jokinen, T., Järvinen, E., Äijälä, M., Kangasluoma, J., Hakala, J., Aalto, P. P., Paasonen, P., Mikkilä, J., Vanhanen, J., Aalto, J., Hakola, H., Makkonen, U., Ruuskanen, T., Mauldin, R. L., Duplissy, J., Vehkamäki, H., Bäck, J., Kortelainen, A., Riipinen, I., Kurtén, T., Johnston, M. V., Smith, J. N., Ehn, M., Mentel, T. F., Lehtinen, K. E. J., Laaksonen, A., Kerminen, V.-M., and Worsnop, D. R.: Direct Observations of Atmospheric Aerosol Nucleation, Science, 339, 943–946, https://doi.org/10.1126/science.1227385, 2013.

Kürten, A., Rondo, L., Ehrhart, S., and Curtius, J.: Calibration of a Chemical Ionization Mass Spectrometer for the Measurement of Gaseous Sulfuric Acid, J. Phys. Chem. A, 116, 6375–6386, https://doi.org/10.1021/jp212123n, 2012.

Lai, S., Qi, X., Huang, X., Lou, S., Chi, X., Chen, L., Liu, C., Liu, Y., Yan, C., Li, M., Liu, T., Nie, W., Kerminen, V.-M., Petäjä, T., Kulmala, M., and Ding, A.: New particle formation induced by anthropogenic–biogenic interactions on the southeastern Tibetan Plateau, Atmospheric Chem. Phys., 24, 2535–2553, https://doi.org/10.5194/acp-24-2535-2024, 2024.

Lehtipalo, K., Yan, C., Dada, L., Bianchi, F., Xiao, M., Wagner, R., Stolzenburg, D., Ahonen, L. R., Amorim, A., Baccarini, A., Bauer, P. S., Baumgartner, B., Bergen, A., Bernhammer, A.-K., Breitenlechner, M., Brilke, S., Buchholz, A., Mazon, S. B., Chen, D., Chen, X., Dias, A., Dommen, J., Draper, D. C., Duplissy, J., Ehn, M., Finkenzeller, H., Fischer, L., Frege, C., Fuchs, C., Garmash, O., Gordon, H., Hakala, J., He, X., Heikkinen, L., Heinritzi, M., Helm, J. C., Hofbauer, V., Hoyle, C. R., Jokinen, T., Kangasluoma, J., Kerminen, V.-M., Kim, C., Kirkby, J., Kontkanen, J., Kürten, A., Lawler, M. J., Mai, H., Mathot, S., Mauldin, R. L., Molteni, U., Nichman, L., Nie, W., Nieminen, T., Ojdanic, A., Onnela, A., Passananti, M., Petäjä, T., Piel, F., Pospisilova, V., Quéléver, L. L. J., Rissanen, M. P., Rose, C., Sarnela, N., Schallhart, S., Schuchmann, S., Sengupta, K., Simon, M., Sipilä, M., Tauber, C., Tomé, A., Tröstl, J., Väisänen, O., Vogel, A. L., Volkamer, R., Wagner, A. C., Wang, M., Weitz, L., Wimmer, D., Ye, P., Ylisirniö, A., Zha, Q., Carslaw, K. S., Curtius, J., Donahue, N. M., Flagan, R. C., Hansel, A., Riipinen, I., Virtanen, A., Winkler, P. M., Baltensperger, U., Kulmala, M., and Worsnop, D. R.: Multicomponent new particle formation from sulfuric acid, ammonia, and biogenic vapors, Sci Adv, 4, eaau5363, https://doi.org/10.1126/sciadv.aau5363, 2018.

Li, H., Riva, M., Rantala, P., Heikkinen, L., Daellenbach, K., Krechmer, J. E., Flaud, P.-M., Worsnop, D., Kulmala, M., Villenave, E., Perraudin, E., Ehn, M., and Bianchi, F.: Terpenes and their oxidation products in the French Landes forest: insights from Vocus PTR-TOF measurements, Atmospheric Chem. Phys., 20, 1941–1959, https://doi.org/10.5194/acp-20-1941-2020, 2020.

Liu, Y., Nie, W., Li, Y., Ge, D., Liu, C., Xu, Z., Chen, L., Wang, T., Wang, L., Sun, P., Qi, X., Wang, J., Xu, Z., Yuan, J., Yan, C., Zhang, Y., Huang, D., Wang, Z., Donahue, N. M., Worsnop, D., Chi, X., Ehn, M., and Ding, A.: Formation of condensable organic vapors from anthropogenic and biogenic volatile organic compounds (VOCs) is strongly perturbed by NO_x in eastern China, Atmospheric Chem. Phys., 21, 14789–14814, https://doi.org/10.5194/acp-21-14789-2021, 2021.

Liu, Y., Nie, W., Qi, X., Li, Y., Xu, T., Liu, C., Ge, D., Chen, L., Niu, G., Wang, J., Yang, L., Wang, L., Zhu, C., Wang, J., Zhang, Y., Liu, T., Zha, Q., Yan, C., Ye, C., Zhang, G., Hu, R., Huang, R.-J., Chi, X., Zhu, T., and Ding, A.: The Pivotal Role of Heavy Terpenes and Anthropogenic Interactions in New Particle Formation on the Southeastern Qinghai-Tibet Plateau, Environ. Sci. Technol., 58, 19748–19761, https://doi.org/10.1021/acs.est.4c04112, 2024.

Luo, Y., Garmash, O., Li, H., Graeffe, F., Praplan, A. P., Liikanen, A., Zhang, Y., Meder, M., Peräkylä, O., Peñuelas, J., Yáñez-Serrano, A. M., and Ehn, M.: Oxidation product characterization from ozonolysis of the diterpene *ent*-kaurene, Atmospheric Chem. Phys., 22, 5619–5637, https://doi.org/10.5194/acp-22-5619-2022, 2022.

Luo, Y., Thomsen, D., Iversen, E. M., Roldin, P., Skønager, J. T., Li, L., Priestley, M., Pedersen, H. B., Hallquist, M., Bilde, M., Glasius, M., and Ehn, M.: Formation and temperature dependence of highly oxygenated organic molecules (HOMs) from Δ^3-carene ozonolysis, Atmospheric Chem. Phys., 24, 9459–9473, https://doi.org/10.5194/acp-24-9459-2024, 2024.

https://doi.org/10.5194/egusphere-2026-2773
Preprint. Discussion started: 15 July 2026

Mohr, C., Thornton, J. A., Heitto, A., Lopez-Hilfiker, F. D., Lutz, A., Riipinen, I., Hong, J., Donahue, N. M., Hallquist, M., Petäjä, T., Kulmala, M., and Yli-Juuti, T.: Molecular identification of organic vapors driving atmospheric nanoparticle growth, Nat. Commun., 10, 4442, https://doi.org/10.1038/s41467-019-12473-2, 2019.

Neefjes, I., Laapas, M., Liu, Y., Médus, E., Miettunen, E., Ahonen, L., Quéléver, L., Aalto, J., Bäck, J., Kerminen, V.-M., Lampilahti, J., Luoma, K., Mäki, M., Mammarella, I., Petäjä, T., Räty, M., Sarnela, N., Ylivinkka, I., Hakala, S., Kulmala, M., Nieminen, T., and Lintunen, A.: 25 years of atmospheric and ecosystem measurements in a boreal forest — Seasonal variation and responses to warm and dry years, Boreal Environ. Res., 27, 1–31, 2022.

Nie, W., Yan, C., Yang, L., Roldin, P., Liu, Y., Vogel, A. L., Molteni, U., Stolzenburg, D., Finkenzeller, H., Amorim, A., Bianchi, F., Curtius, J., Dada, L., Draper, D. C., Duplissy, J., Hansel, A., He, X.-C., Hofbauer, V., Jokinen, T., Kim, C., Lehtipalo, K., Nichman, L., Mauldin, R. L., Makhmutov, V., Mentler, B., Mizelli-Ojdanic, A., Petäjä, T., Quéléver, L. L. J., Schallhart, S., Simon, M., Tauber, C., Tomé, A., Volkamer, R., Wagner, A. C., Wagner, R., Wang, M., Ye, P., Li, H., Huang, W., Qi, X., Lou, S., Liu, T., Chi, X., Dommen, J., Baltensperger, U., El Haddad, I., Kirkby, J., Worsnop, D., Kulmala, M., Donahue, N. M., Ehn, M., and Ding, A.: NO at low concentration can enhance the formation of highly oxygenated biogenic molecules in the atmosphere, Nat. Commun, 14, 3347, https://doi.org/10.1038/s41467-023-39066-4, 2023.

O'Dowd, C. D., Aalto, P., Hmeri, K., Kulmala, M., and Hoffmann, T.: Atmospheric particles from organic vapours, Nature, 416, 497–498, https://doi.org/10.1038/416497a, 2002.

Peräkylä, O., Riva, M., Heikkinen, L., Quéléver, L., Roldin, P., and Ehn, M.: Experimental investigation into the volatilities of highly oxygenated organic molecules (HOMs), Atmospheric Chem. Phys., 20, 649–669, https://doi.org/10.5194/acp-20-649-2020, 2020.

Peräkylä, O., Berndt, T., Franzon, L., Hasan, G., Meder, M., Valiev, R. R., Daub, C. D., Varelas, J. G., Geiger, F. M., Thomson, R. J., Rissanen, M., Kurtén, T., and Ehn, M.: Large Gas-Phase Source of Esters and Other Accretion Products in the Atmosphere, J. Am. Chem. Soc., 145, 7780–7790, https://doi.org/10.1021/jacs.2c10398, 2023.

Petäjä, T., Tabakova, K., Manninen, A., Ezhova, E., O'Connor, E., Moisseev, D., Sinclair, V. A., Backman, J., Levula, J., Luoma, K., Virkkula, A., Paramonov, M., Räty, M., Äijälä, M., Heikkinen, L., Ehn, M., Sipilä, M., Yli-Juuti, T., Virtanen, A., Ritsche, M., Hickmon, N., Pulik, G., Rosenfeld, D., Worsnop, D. R., Bäck, J., Kulmala, M., and Kerminen, V.-M.: Influence of biogenic emissions from boreal forests on aerosol–cloud interactions, Nat. Geosci., 15, 42–47, https://doi.org/10.1038/s41561-021-00876-0, 2022.

Praske, E., Otkjær, R. V., Crounse, J. D., Hethcox, J. C., Stoltz, B. M., Kjaergaard, H. G., and Wennberg, P. O.: Atmospheric autoxidation is increasingly important in urban and suburban North America, Proc. Natl. Acad. Sci., 115, 64–69, https://doi.org/10.1073/pnas.1715540115, 2018.

Pullinen, I., Schmitt, S., Kang, S., Sarrafzadeh, M., Schlag, P., Andres, S., Kleist, E., Mentel, T. F., Rohrer, F., Springer, M., Tillmann, R., Wildt, J., Wu, C., Zhao, D., Wahner, A., and Kiendler-Scharr, A.: Impact of NO_x on secondary organic aerosol (SOA) formation from α-pinene and β-pinene photooxidation: the role of highly oxygenated organic nitrates, Atmospheric Chem. Phys., 20, 10125–10147, https://doi.org/10.5194/acp-20-10125-2020, 2020.

Quéléver, L. L. J., Kristensen, K., Normann Jensen, L., Rosati, B., Teiwes, R., Daellenbach, K. R., Peräkylä, O., Roldin, P., Bossi, R., Pedersen, H. B., Glasius, M., Bilde, M., and Ehn, M.: Effect of temperature on the formation of highly oxygenated organic molecules (HOMs) from alpha-pinene ozonolysis, Atmospheric Chem. Phys., 19, 7609–7625, https://doi.org/10.5194/acp-19-7609-2019, 2019.

https://doi.org/10.5194/egusphere-2026-2773
Preprint. Discussion started: 15 July 2026

Rantala, P., Aalto, J., Taipale, R., Ruuskanen, T. M., and Rinne, J.: Annual cycle of volatile organic compound exchange between a boreal pine forest and the atmosphere, Biogeosciences, 12, 5753–5770, https://doi.org/10.5194/bg-12-5753-2015, 2015.

Riccobono, F., Schobesberger, S., Scott, C. E., Dommen, J., Ortega, I. K., Rondo, L., Almeida, J., Amorim, A., Bianchi, F., Breitenlechner, M., David, A., Downard, A., Dunne, E. M., Duplissy, J., Ehrhart, S., Flagan, R. C., Franchin, A., Hansel, A., Junninen, H., Kajos, M., Keskinen, H., Kupc, A., Kürten, A., Kvashin, A. N., Laaksonen, A., Lehtipalo, K., Makhmutov, V., Mathot, S., Nieminen, T., Onnela, A., Petäjä, T., Praplan, A. P., Santos, F. D., Schallhart, S., Seinfeld, J. H., Sipilä, M., Spracklen, D. V., Stozhkov, Y., Stratmann, F., Tomé, A., Tsagkogeorgas, G., Vaattovaara, P., Viisanen, Y., Vrtala, A., Wagner, P. E., Weingartner, E., Wex, H., Wimmer, D., Carslaw, K. S., Curtius, J., Donahue, N. M., Kirkby, J., Kulmala, M., Worsnop, D. R., and Baltensperger, U.: Oxidation Products of Biogenic Emissions Contribute to Nucleation of Atmospheric Particles, Science, 344, 717–721, https://doi.org/10.1126/science.1243527, 2014.

Rissanen, M. P., Mikkilä, J., Iyer, S., and Hakala, J.: Multi-scheme chemical ionization inlet (MION) for fast switching of reagent ion chemistry in atmospheric pressure chemical ionization mass spectrometry (CIMS) applications, Atmospheric Meas. Tech., 12, 6635–6646, https://doi.org/10.5194/amt-12-6635-2019, 2019.

Roldin, P., Ehn, M., Kurtén, T., Olenius, T., Rissanen, M. P., Sarnela, N., Elm, J., Rantala, P., Hao, L., Hyttinen, N., Heikkinen, L., Worsnop, D. R., Pichelstorfer, L., Xavier, C., Clusius, P., Öström, E., Petäjä, T., Kulmala, M., Vehkamäki, H., Virtanen, A., Riipinen, I., and Boy, M.: The role of highly oxygenated organic molecules in the Boreal aerosol-cloud-climate system, Nat. Commun., 10, 4370, https://doi.org/10.1038/s41467-019-12338-8, 2019.

Schobesberger, S., Junninen, H., Bianchi, F., Lönn, G., Ehn, M., Lehtipalo, K., Dommen, J., Ehrhart, S., Ortega, I. K., Franchin, A., Nieminen, T., Riccobono, F., Hutterli, M., Duplissy, J., Almeida, J., Amorim, A., Breitenlechner, M., Downard, A. J., Dunne, E. M., Flagan, R. C., Kajos, M., Keskinen, H., Kirkby, J., Kupc, A., Kürten, A., Kurtén, T., Laaksonen, A., Mathot, S., Onnela, A., Praplan, A. P., Rondo, L., Santos, F. D., Schallhart, S., Schnitzhofer, R., Sipilä, M., Tomé, A., Tsagkogeorgas, G., Vehkamäki, H., Wimmer, D., Baltensperger, U., Carslaw, K. S., Curtius, J., Hansel, A., Petäjä, T., Kulmala, M., Donahue, N. M., and Worsnop, D. R.: Molecular understanding of atmospheric particle formation from sulfuric acid and large oxidized organic molecules, Proc. Natl. Acad. Sci., 110, 17223–17228, https://doi.org/10.1073/pnas.1306973110, 2013.

Shen, J., Russell, D. M., DeVivo, J., Kunkler, F., Baalbaki, R., Mentler, B., Scholz, W., Yu, W., Caudillo-Plath, L., Sommer, E., Ahongshangbam, E., Alfaouri, D., Almeida, J., Amorim, A., Beck, L. J., Beckmann, H., Berntheusel, M., Bhattacharyya, N., Canagaratna, M. R., Chassaing, A., Cruz-Simbron, R., Dada, L., Duplissy, J., Gordon, H., Granzin, M., Große Schute, L., Heinritzi, M., Iyer, S., Klebach, H., Krüger, T., Kürten, A., Lampimäki, M., Liu, L., Lopez, B., Martinez, M., Morawiec, A., Onnela, A., Peltola, M., Rato, P., Reza, M., Richter, S., Rörup, B., Sebastian, M. K., Simon, M., Surdu, M., Tamme, K., Thakur, R. C., Tomé, A., Tong, Y., Top, J., Umo, N. S., Unfer, G., Vettikkat, L., Weissbacher, J., Xenofontos, C., Yang, B., Zauner-Wieczorek, M., Zhang, J., Zheng, Z., Baltensperger, U., Christoudias, T., Flagan, R. C., El Haddad, I., Junninen, H., Möhler, O., Riipinen, I., Rohner, U., Schobesberger, S., Volkamer, R., Winkler, P. M., Hansel, A., Lehtipalo, K., Donahue, N. M., Lelieveld, J., Harder, H., Kulmala, M., Worsnop, D. R., Kirkby, J., Curtius, J., and He, X.-C.: New particle formation from isoprene under upper-tropospheric conditions, Nature, 636, 115–123, https://doi.org/10.1038/s41586-024-08196-0, 2024.

Stolzenburg, D., Fischer, L., Vogel, A. L., Heinritzi, M., Schervish, M., Simon, M., Wagner, A. C., Dada, L., Ahonen, L. R., Amorim, A., Baccarini, A., Bauer, P. S., Baumgartner, B., Bergen, A., Bianchi, F., Breitenlechner, M., Brilke, S., Buenrostro Mazon, S., Chen, D., Dias, A., Draper, D. C., Duplissy, J., El Haddad, I., Finkenzeller, H., Frege, C., Fuchs, C., Garmash, O., Gordon, H., He, X., Helm, J., Hofbauer, V., Hoyle, C. R., Kim, C., Kirkby, J., Kontkanen, J., Kürten, A., Lampilahti, J., Lawler, M., Lehtipalo, K., Leiminger, M., Mai, H., Mathot, S., Mentler, B., Molteni, U., Nie, W., Nieminen, T., Nowak, J. B., Ojdanic, A., Onnela, A., Passananti, M., Petäjä, T., Quéléver, L. L. J., Rissanen, M. P., Sarnela, N., Schallhart, S., Tauber, C., Tomé, A., Wagner, R., Wang, M., Weitz, L., Wimmer, D., Xiao, M., Yan, C., Ye, P., Zha, Q., Baltensperger, U., Curtius, J., Dommen, J., Flagan, R. C., Kulmala, M., Smith, J. N., Worsnop, D. R., Hansel, A., Donahue, N. M., and Winkler, P. M.:

Rapid growth of organic aerosol nanoparticles over a wide tropospheric temperature range, Proc. Natl. Acad. Sci., 115, 9122–9127, https://doi.org/10.1073/pnas.1807604115, 2018.

Sulo, J., Sarnela, N., Kontkanen, J., Ahonen, L., Paasonen, P., Laurila, T., Jokinen, T., Kangasluoma, J., Junninen, H., Sipilä, M., Petäjä, T., Kulmala, M., and Lehtipalo, K.: Long-term measurement of sub-3 nm particles and their precursor gases in the boreal forest, Atmospheric Chem. Phys., 21, 695–715, https://doi.org/10.5194/acp-21-695-2021, 2021.

Taipale, R., Ruuskanen, T. M., Rinne, J., Kajos, M. K., Hakola, H., Pohja, T., and Kulmala, M.: Technical Note: Quantitative long-term measurements of VOC concentrations by PTR-MS – measurement, calibration, and volume mixing ratio calculation methods, Atmospheric Chem. Phys., 8, 6681–6698, https://doi.org/10.5194/acp-8-6681-2008, 2008.

Tröstl, J., Chuang, W. K., Gordon, H., Heinritzi, M., Yan, C., Molteni, U., Ahlm, L., Frege, C., Bianchi, F., Wagner, R., Simon, M., Lehtipalo, K., Williamson, C., Craven, J. S., Duplissy, J., Adamov, A., Almeida, J., Bernhammer, A.-K., Breitenlechner, M., Brilke, S., Dias, A., Ehrhart, S., Flagan, R. C., Franchin, A., Fuchs, C., Guida, R., Gysel, M., Hansel, A., Hoyle, C. R., Jokinen, T., Junninen, H., Kangasluoma, J., Keskinen, H., Kim, J., Krapf, M., Kürten, A., Laaksonen, A., Lawler, M., Leiminger, M., Mathot, S., Möhler, O., Nieminen, T., Onnela, A., Petäjä, T., Piel, F. M., Miettinen, P., Rissanen, M. P., Rondo, L., Sarnela, N., Schobesberger, S., Sengupta, K., Sipilä, M., Smith, J. N., Steiner, G., Tomè, A., Virtanen, A., Wagner, A. C., Weingartner, E., Wimmer, D., Winkler, P. M., Ye, P., Carslaw, K. S., Curtius, J., Dommen, J., Kirkby, J., Kulmala, M., Riipinen, I., Worsnop, D. R., Donahue, N. M., and Baltensperger, U.: The role of low-volatility organic compounds in initial particle growth in the atmosphere, Nature, 533, 527–531, https://doi.org/10.1038/nature18271, 2016.

Vana, M., Komsaare, K., Hõrrak, U., Mirme, S., Nieminen, T., Kontkanen, J., Manninen, H. E., Petäjä, T., Noe, S. M., and Kulmala, M.: Characteristics of new-particle formation at three SMEAR stations, Boreal Environ. Res., 21, 345–362, 2016.

Wang, H., Liu, X., Wu, C., and Lin, G.: Regional to global distributions, trends, and drivers of biogenic volatile organic compound emission from 2001 to 2020, Atmospheric Chem. Phys., 24, 3309–3328, https://doi.org/10.5194/acp-24-3309-2024, 2024a.

Wang, H., Liu, X., Wu, C., and Lin, G.: Regional to global distributions, trends, and drivers of biogenic volatile organic compound emission from 2001 to 2020, Atmospheric Chem. Phys., 24, 3309–3328, https://doi.org/10.5194/acp-24-3309-2024, 2024b.

Yan, C., Nie, W., Äijälä, M., Rissanen, M. P., Canagaratna, M. R., Massoli, P., Junninen, H., Jokinen, T., Sarnela, N., Häme, S. A. K., Schobesberger, S., Canonaco, F., Yao, L., Prévôt, A. S. H., Petäjä, T., Kulmala, M., Sipilä, M., Worsnop, D. R., and Ehn, M.: Source characterization of highly oxidized multifunctional compounds in a boreal forest environment using positive matrix factorization, Atmospheric Chem. Phys., 16, 12715–12731, https://doi.org/10.5194/acp-16-12715-2016, 2016.

Yan, C., Nie, W., Vogel, A. L., Dada, L., Lehtipalo, K., Stolzenburg, D., Wagner, R., Rissanen, M. P., Xiao, M., Ahonen, L., Fischer, L., Rose, C., Bianchi, F., Gordon, H., Simon, M., Heinritzi, M., Garmash, O., Roldin, P., Dias, A., Ye, P., Hofbauer, V., Amorim, A., Bauer, P. S., Bergen, A., Bernhammer, A.-K., Breitenlechner, M., Brilke, S., Buchholz, A., Mazon, S. B., Canagaratna, M. R., Chen, X., Ding, A., Dommen, J., Draper, D. C., Duplissy, J., Frege, C., Heyn, C., Guida, R., Hakala, J., Heikkinen, L., Hoyle, C. R., Jokinen, T., Kangasluoma, J., Kirkby, J., Kontkanen, J., Kürten, A., Lawler, M. J., Mai, H., Mathot, S., Mauldin, R. L., Molteni, U., Nichman, L., Nieminen, T., Nowak, J., Ojdanic, A., Onnela, A., Pajunoja, A., Petäjä, T., Piel, F., Quéléver, L. L. J., Sarnela, N., Schallhart, S., Sengupta, K., Sipilä, M., Tomé, A., Tröstl, J., Väisänen, O., Wagner, A. C., Ylisirniö, A., Zha, Q., Baltensperger, U., Carslaw, K. S., Curtius, J., Flagan, R. C., Hansel, A., Riipinen, I., Smith, J. N., Virtanen, A., Winkler, P. M., Donahue, N. M., Kerminen, V.-M., Kulmala, M., Ehn, M., and Worsnop, D. R.: Size-dependent influence of NOx on the growth rates of organic aerosol particles, Sci Adv, 6, eaay4945, https://doi.org/10.1126/sciadv.aay4945, 2020.

https://doi.org/10.5194/egusphere-2026-2773
Preprint. Discussion started: 15 July 2026

Yan, C., Yin, R., Lu, Y., Dada, L., Yang, D., Fu, Y., Kontkanen, J., Deng, C., Garmash, O., Ruan, J., Baalbaki, R., Schervish, M., Cai, R., Bloss, M., Chan, T., Chen, T., Chen, Q., Chen, X., Chen, Y., Chu, B., Dällenbach, K., Foreback, B., He, X., Heikkinen, L., Jokinen, T., Junninen, H., Kangasluoma, J., Kokkonen, T., Kurppa, M., Lehtipalo, K., Li, H., Li, H., Li, X., Liu, Y., Ma, Q., Paasonen, P., Rantala, P., Pileci, R. E., Rusanen, A., Sarnela, N., Simonen, P., Wang, S., Wang, W., Wang, Y., Xue, M., Yang, G., Yao, L., Zhou, Y., Kujansuu, J., Petäjä, T., Nie, W., Ma, Y., Ge, M., He, H., Donahue, N. M., Worsnop, D. R., Kerminen, V.-M., Wang, L., Liu, Y., Zheng, J., Kulmala, M., Jiang, J., and Bianchi, F.: The Synergistic Role of Sulfuric Acid, Bases, and Oxidized Organics Governing New-Particle Formation in Beijing, Geophys. Res. Lett., 48, e2020GL091944, https://doi.org/10.1029/2020GL091944, 2021.

Yin, J., Liu, Y., Nie, W., Yan, C., Zha, Q., Li, Y., Ge, D., Liu, C., Zhu, C., Chi, X., and Ding, A.: Unveiling the formation of atmospheric oxygenated organic molecules under anthropogenic–biogenic interactions: insights from binned positive matrix factorization on multi-subrange mass spectra, Atmospheric Chem. Phys., 25, 13279–13297, https://doi.org/10.5194/acp-25-13279-2025, 2025.

Ylivinkka, I., Mikkelsen, M. K., Nissinen, A., Pennacchio, L., Strömberg, J., Saranko, O., Utriainen, L., Valiati, R., Aalto, J., Banerji, S., Heikkinen, L., Lintunen, A., Luoma, K., Peräkylä, O., Sarnela, N., Taipale, D., Taipale, R., Thomas, S. J., Zhang, X., and Kulmala, M.: Intervention of pollution episodes from nearby sawmills to ecosystem-atmosphere interactions studied in a boreal forest at SMEAR II, Boreal Environ. Res., https://doi.org/10.60910/BER2025.727E-SW95, 2025.

Zha, Q., Aliaga, D., Krejci, R., Sinclair, V. A., Wu, C., Ciarelli, G., Scholz, W., Heikkinen, L., Partoll, E., Gramlich, Y., Huang, W., Leiminger, M., Enroth, J., Peräkylä, O., Cai, R., Chen, X., Koenig, A. M., Velarde, F., Moreno, I., Petäjä, T., Artaxo, P., Laj, P., Hansel, A., Carbone, S., Kulmala, M., Andrade, M., Worsnop, D., Mohr, C., and Bianchi, F.: Oxidized organic molecules in the tropical free troposphere over Amazonia, Natl. Sci. Rev., 11, nwad138, https://doi.org/10.1093/nsr/nwad138, 2024.

Zhang, Y., Peräkylä, O., Yan, C., Heikkinen, L., Äijälä, M., Daellenbach, K. R., Zha, Q., Riva, M., Garmash, O., Junninen, H., Paatero, P., Worsnop, D., and Ehn, M.: A novel approach for simple statistical analysis of high-resolution mass spectra, Atmospheric Meas. Tech., 12, 3761–3776, https://doi.org/10.5194/amt-12-3761-2019, 2019.

Zhao, B., Donahue, N. M., Zhang, K., Mao, L., Shrivastava, M., Ma, P.-L., Shen, J., Wang, S., Sun, J., Gordon, H., Tang, S., Fast, J., Wang, M., Gao, Y., Yan, C., Singh, B., Li, Z., Huang, L., Lou, S., Lin, G., Wang, H., Jiang, J., Ding, A., Nie, W., Qi, X., Chi, X., and Wang, L.: Global variability in atmospheric new particle formation mechanisms, Nature, 1–8, https://doi.org/10.1038/s41586-024-07547-1, 2024.

Zhao, J., Ortega, J., Chen, M., McMurry, P. H., and Smith, J. N.: Dependence of particle nucleation and growth on high-molecular-weight gas-phase products during ozonolysis of α-pinene, Atmospheric Chem. Phys., 13, 7631–7644, https://doi.org/10.5194/acp-13-7631-2013, 2013.

Ziemann, P. J. and Atkinson, R.: Kinetics, products, and mechanisms of secondary organic aerosol formation, Chem. Soc. Rev., 41, 6582–6605, https://doi.org/10.1039/C2CS35122F, 2012.